Journal of Controlled Release 370 (2024) 239–255

Contents lists available at ScienceDirect

Journal of Controlled Release

journal homepage: www.elsevier.com/locate/jconrel

Lipo-Xenopeptide Polyplexes for CRISPR/Cas9 based Gene editing at ultra-low dose

Janin Germer [a], Anna-Lina Lessl [a], Jana Pöhmerer [a], Melina Grau [a], Eric Weidinger [a], Miriam Höhn [a], Mina Yazdi [a], Martino Alfredo Cappelluti [b], Angelo Lombardo [b,c], Ulrich Lächelt [d,e], Ernst Wagner [a,d,f,*]

[a] Pharmaceutical Biotechnology, Department of Pharmacy, Ludwig-Maximilians-Universität Munich, Butenandtstrasse 5-13, Munich 81377, Germany
[b] San Raffaele Telethon Institute for Gene Therapy, IRCCS San Raffaele Scientific Institute, Milan 20132, Italy
[c] Vita-Salute San Raffaele University, Milan 20132, Italy
[d] Center for Nanoscience (CeNS), LMU Munich, Munich 80799, Germany
[e] Department of Pharmaceutical Sciences, University of Vienna, Josef-Holaubek-Platz 2, Vienna 1090, Austria
[f] CNATM - Cluster for Nucleic Acid Therapeutics Munich, Germany

ARTICLE INFO

Keywords:
CRISPR Cas9
Delivery
Genome editing
Lipid nanoparticle
mRNA
Polyplexes
Xenopeptide

ABSTRACT

Double pH-responsive xenopeptide carriers containing succinoyl tetraethylene pentamine (Stp) and lipo amino fatty acids (LAFs) were evaluated for CRISPR/Cas9 based genome editing. Different carrier topologies, variation of LAF/Stp ratios and LAF types as Cas9 mRNA/sgRNA polyplexes were screened in three different reporter cell lines using three different genomic targets (*Pcsk9*, eGFP, *mdx* exon 23). One U-shaped and three bundle (B2)-shaped lipo-xenopeptides exhibiting remarkable efficiencies were identified. Genome editing potency of top carriers were observed at sub-nanomolar EC_{50} concentrations of 0.4 nM sgRNA and 0.1 nM sgRNA for the top U-shape and top B2 carriers, respectively, even after incubation in full ($\geq$ 90%) serum. Polyplexes co-delivering Cas9 mRNA/sgRNA with a single stranded DNA template for homology directed gene editing resulted in up to 38% conversion of eGFP to BFP in reporter cells. Top carriers were formulated as polyplexes or lipid nanoparticles (LNPs) for subsequent *in vivo* administration. Formulations displayed long-term physicochemical and functional stability upon storage at 4 °C. Importantly, intravenous administration of polyplexes or LNPs mediated *in vivo* editing of the dystrophin gene, triggering mRNA exon 23 splicing modulation in dystrophin-expressing cardiac muscle, skeletal muscle and brain tissue.

1. Introduction

At current >32 gene therapies and > 28 RNA therapies have been approved as medical drugs [1]. Due to their superior *in vivo* potency, viral vectors such as AAV pioneered the development of novel *in vivo* gene therapies. Nevertheless, a continuous development of synthetic, non-viral nucleic acid delivery systems over five decades resulted in the recent global medical impact of lipid nanoparticles (LNPs) in SARS-CoV-2 mRNA vaccines [2]. Additionally, LNPs were approved as hepatocyte-targeted siRNA drug Onpattro for treatment of hereditary transthyretin amyloidosis [3]. The chemical space of synthetic carriers [4,5] ranges from small cationic lipids applied in lipoplexes [6–10] and lipid nanoparticles (LNPs) [3,10–17], over medium-sized sequence-defined xenopeptides to macromolecular polycations applied in polyplexes and polymer micelles [18–36]. In general, the efficacies of synthetic vectors are still moderate on nanoparticle basis, but can be compensated by enhanced nanoparticle dose, as well tolerated formulations can be produced in precise form and at large scale. In recent years numerous novel synthetic mRNA carriers have been developed [37–39]. The transient expression of mRNA might be seen as weakness for some application. However, for the Nobel Prize-winning CRISPR/Cas9 technology, short-term function is clearly advantageous both in terms of genetic safety and immunogenicity reasons [40]. The first *ex vivo* CRISPR/Cas9 application, CASGEVY™, recently received the approved drug status for treatment of sickle cell anemia [41,42]; electroporation is applied for intracellular delivery of Cas9/sgRNA ribonucleoproteins

* Corresponding author at: Pharmaceutical Biotechnology, Department of Pharmacy, Ludwig-Maximilians-Universität Munich, Butenandtstrasse 5-13, Munich 81377, Germany
E-mail address: ernst.wagner@lmu.de (E. Wagner).

https://doi.org/10.1016/j.jconrel.2024.04.037
Received 18 January 2024; Received in revised form 17 April 2024; Accepted 22 April 2024
Available online 27 April 2024

(RNPs) into hematopoietic stem cells. The *in vivo* LNP therapy NTLA-2001, transferring Cas9 mRNA/sgRNA into liver hepatocytes, just entered advanced clinical evaluation in global phase 3 studies [43]. Nevertheless, for applications beyond local administration or delivery into hepatocytes, efficient and safe delivery of the Cas9 system remains a challenge.

The CRISPR/Cas9 system consisting of the RNA-guided endonuclease Cas9, a single guide RNA (sgRNA) and – optionally - donor DNA in case of homology-directed recombination repair (HDR) can be delivered with different non-viral formats [44,45]. Constructs encoding the nuclease based on pDNA, on mRNA co-delivered with sgRNA, or direct delivery of the recombinant Cas9 protein with sgRNA as RNP formulation have been utilized [46–48]. Starting point of the current study was a novel design strategy of sequence-defined xenopeptide carrier libraries by chemical evolution [49–52]. Notably, different nucleic acid cargos possess differing delivery demands, due to diverse physicochemical properties (lengths and type of nucleic acid) and diverging biological functions and locations such as the cytosol or nucleus [36,53]. Optimized carriers for Cas9/sgRNA RNPs delivery with high efficiency at sub-nanomolar concentration had been identified [50,51] that however display only moderate RNA delivery potential (our unpublished data). A recent carrier library of double pH-responsive lipo-xenopeptides comprising ionizable lipo amino fatty acid (LAF) domains includes excellent RNA carriers with efficacy at very low dose, comparable to viral vectors, when formulated into either mRNA polyplexes [52] or LNPs [54]. Different library members trigger potent pDNA transfer, others present effective siRNA delivery [52]. As demonstrated in the following, potency of mRNA carriers and formulations may but need not necessarily be predictive for Cas9 mRNA/sgRNA delivery. Cas9mRNA (4.5 kb) is more than twice as large as luciferase mRNA (1.9 kb), and co-delivery with smaller sgRNA, and ideally also ssDNA for homology directed repair (HDR) makes it a more demanding cargo. To address this question, we screened in the current work the new LAF lipo-xenopeptide library for dual formulation of pDNA and mRNA, for Cas9 mRNA/sgRNA polyplex or LNP formulation, and present identified potent carriers for their application in genome editing *in vitro* and *in vivo*.

2. Experimental section/methods

2.1. Materials

Cas9 mRNA, *i.e.* CleanCap® Cas9 mRNA (5moU), Luc mRNA, *i.e.* CleanCap® FLuc mRNA (5moU) and mCherry mRNA, *i.e.*, CleanCap® mCherry mRNA (5moU) were obtained from Trilink Biotechnologies (San Diego, CA, USA). Plasmid pEGFP-N1 (encoding eGFP under control of cytomegalovirus promotor and enhancer) was obtained from Clontech Laboratories; Inc. (now Takara Bio USA, Inc., San Jose, CA, USA). Single guide RNA (sgRNA) sgPcsk9, substituted with 2'-*O*-methyl residues and phosphorothioate backbone modifications [55,56], was purchased from AxoLabs GmbH (Kulmbach, Germany). Other sgRNA have phosphorothioated 2'-*O*-methyl modifications on the first 3 and penultimate 3 RNA bases and were purchased from Integrated DNA Technologies (IDT; Coralville, Iowa, USA). The sequences and modification pattern are shown in **Table S1**. Cas9 protein expression and purification was performed in house as previously described [57]. HEPES was obtained from Biomol (Hamburg, Germany), glucose as well as disodium ethylenediaminetetraacetic acid (EDTA) from Merck (Darmstadt, Germany). Agarose BioReagent – low EEO and RNase-free water were purchased from Sigma Aldrich (Munich, Germany), and heparin-sodium salt 5000 I.U. mL^{-1} from B. Braun SE (Melsungen, Germany). All cell culture consumables were obtained from Faust Lab Science (Klettgau, Germany). Cell culture media, fetal bovine serum (FBS), trypsin/EDTA, antibiotics, as well as paraformaldehyde (PFA) were purchased from PANBiotech (Aidenbach, Germany) and Sigma Aldrich (Munich, Germany). Cell culture 5× lysis buffer, GoTaq^R Hot Start polymerase, and D-luciferin sodium salt were obtained from Promega (Walldorf, Germany). 3-(4,5-dimethylthiazol-2-yl)-2,5-diphenyiltetrazolium bromide (MTT), 4′,6-diamidino-2-phenylindole (DAPI), dithiothreitol (DTT), adenosine 5′-triphosphate (ATP) disodium salt trihydrate, coenzyme A trilithium salt, and propidium iodide from Sigma-Aldrich (Munich, Germany). Lipofectamine™ MessengerMAX™, Quant-iT™ RiboGreen RNA Assay-Kit, RNAlater™ Stabilization Solution as well as rhodamin-phalloidin (Invitrogen) were purchased from Thermo Fisher Scientific (Schwerte, Germany). Peqlab peqGOLD, total RNA Kit qScript™, DNA Ladder 1 kb, cDNA SuperMix (QuantaBio), RNASolv and GelRed 10,000× were purchased from VWR (Darmstadt, Germany). QIAmp DNA Mini Kit, QIAquick Gel Extraction kit and QIAquick PCR purification Kit were purchased from QIAGEN (Hilden, Germany). One *Taq*^{R} DNA Polymerase and *Taq*^{R} DNA Polymerase were purchased from NEB (New England Biolabs, Ipswich, Massachusetts, USA). All further solvents and other reagents were purchased from Sigma-Aldrich (Munich, Germany), Iris Biotech (Marktredwitz, Germany), Merck (Darmstadt, Germany), or AppliChem (Darmstadt, Germany). Cholesterol was purchased from Sigma-Aldrich (Munich, Germany). 1,2-Distearoyl-sn-glycero-3-phosphocholine (DSPC), 1,2-dioleoyl-sn-glycero-3-phosphoethanolamine (DOPE) and 1,2-dimyristoyl-rac-glycero-3-methoxypolyethylene glycol-2000 (DMG-PEG 2000) were obtained from Avanti Polar Lipids (Alabaster, AL, USA). The ionizable lipid SM-102 was ordered from Biosynth Carbosynth. Further information regarding materials and methods is provided in the Supporting Information.

2.2. Synthesis of ionizable nucleic acid carriers

The solid phase synthesis of the LAF–Stp carrier library was performed as previously described by Thalmayr et al. [52]. Succinylated branched PEI 25 kDa (succPEI; succinylation degree of 10%) was synthesized and analyzed as described previously [58]. The starting material branched PEI (brPEI) 25 kDa was purchased from Sigma Aldrich (Munich, Germany).

2.3. Polyplex formation

Either Luc mRNA or a combination of Cas9 mRNA and sgRNA at a fixed weight ratio of 1:1 were mixed and diluted in HBG (20 mM of HEPES, 5% (*w/v*) glucose, pH 7.4). The calculated amounts of aminolipid carrier at indicated N/P (nitrogen/phosphate) ratio were diluted in separate tubes of HBG. All secondary amines, terminal amines and the tertiary amines of the carrier structure were considered in the N/P ratio calculations. Equal volumes of nucleic acid solution and aminolipid solution were mixed by rapid pipetting and incubated 40 min at RT in a closed Eppendorf reaction tube. The final concentration of nucleic acid in the polyplex solution was 12.5 μg mL^{-1} (6.25 μg mL^{-1} Cas9 mRNA plus 6.25 μg mL-^{1} sgRNA or 12.5 μg μg mL-^{1} Luc mRNA) for *in vitro* experiments. For *in vivo* experiments polyplexes were mixed achieving a final concentration of 20 μg mL^{-1} (or 67 μg mL^{-1}) and 60 μg mL^{-1} (or 200 μg mL^{-1}) total RNA (Luc mRNA or Cas9 mRNA and sgRNA at weight ratio 1:1) for intravenous and intramuscular application, respectively.

2.4. Lipid nanoparticle (LNP) formation

LNPs of commercially available positive control ionizable lipid SM-102 or the LAF carrier 1621 were formulated by mixing an acidic aqueous phase containing the nucleic acid with an ethanolic phase containing helper lipids and the ionizable lipid by rapid pipetting. The aqueous phase was prepared in citrate buffer (10 mM, pH 4.0) containing either Luc mRNA or a mix of Cas9 mRNA and sgRNA at weight ratio 1:1. The ethanolic phase includes a mixture of the lipidic components at molar ratio of 38.5:10:1.5:50 mol% (Chol:DSPC:PEG-DMG:SM-102) or 47.6:23.8:4.8:23.8 mol% (Chol:DOPE:PEG-DMG:1621) [59] at the N/P ratio of 6 (for SM-102) or 24 (for 1621), respectively. The aqueous nucleic acid solution and ethanolic lipid mixture were mixed at a defined volumetric ratio of 3:1 (lipid mixture: nucleic acid solution) by

rapid pipetting. Following 15 min incubation at RT, the solutions were dialyzed for 2 h against HBG in 1 kDa MWCO tubes at 4 °C. If needed HBG was added to obtain final concentration of 20 μg mL^{-1} and 60 μg mL^{-1} total RNA (Luc mRNA or Cas9 mRNA and sgRNA at weight ratio 1:1) for intravenous and intramuscular application, respectively.

2.5. Cas9 mRNA/sgGFP/ssDNA polyplex formation for eGFP to BFP conversion study

Cas9 mRNA and sgGFP at a fixed weight ratio of 1:1 were mixed with indicated molar ratios of total sgGFP to the single stranded DNA (ssDNA) template (IDT, Coralville, IA, USA) and diluted in HBG. Equal volumes of this nucleic acid solution in HBG and LAF-Stp carrier 1611 solution in HBG were mixed by rapid pipetting resulting in an N/P ratio of 18 and incubated 40 min at RT in a closed Eppendorf reaction tube. The final total concentration of nucleic acid in the polyplex solution was 7.5 μg mL^{-1}.

2.6. Particle size and zeta-potential measurements

Polyplexes and LNPs were formulated in HBG as described above and if needed diluted with HBG to a concentrations of 12.5 μg mL^{-1} total RNA (Cas9 mRNA sgRNA at weight ratio 1:1 or Luc mRNA). Measurements of size and zeta potential were performed with a Zetasizer Nano ZS (Malvern Instruments, Malvern) in a folded capillary cell (DTS1070) by dynamic and electrophoretic laser-light scattering (DLS, ELS). Size and polydispersity index were measured in 80 μL of polyplex or LNP solution using the following instrument settings: equilibration time 30 s, temperature 25 °C, refractive index 1.330, viscosity 0.8872 mPa*s. Samples were measured three times with six sub-runs per measurement. For measurement of the zeta potential, all samples were diluted to 800 μL with HBG directly before measurement. Parameters were identical to the size measurement apart from an equilibration time of 60 s. Three measurements with 15 sub-runs lasting 10 s each were performed, and zeta potentials were calculated by the Smuchowski equation.

2.7. Encapsulation efficiency

The encapsulation efficiency (EE (%)) of LNPs and polyplexes was determined using the Quant - iT™ RiboGreen RNA Assay-Kit (Thermo Fisher Scientific). Polyplexes and LNPs were mixed as above and diluted with 1× TE (10 mM Tris-HCl, 1 mM EDTA, pH 7.5 in RNase-free water) to an mRNA concentration of 2 μg mL^{-1}. 50 μL of the diluted nanoparticles was either mixed with 50 μL of 1 × TE as untreated controls or added to 50 μL of 1 × TE containing 2% (*v*/v) Triton X-100 as treated samples. Additional 250 I.U. mL^{-1} heparin was added for complete dissociation of polyplexes. After a 10 min incubation at 37 °C under constant shaking at 150 rpm and cooling down to RT, 100 μL of RiboGreen reagent 200-fold in 1× TE was added to each sample. Fluorescence was measured after 5 min in a Tecan microplate reader (Spectrafluor Plus, Tecan, Männedorf, Switzerland) at excitation/emission wavelength of 485/535 nm in duplicates. Background was measured with pure HBG in 1× TE, 1× TE supplemented with Triton X-100 for LNP or 1× TE supplemented with Triton X-100 and heparin for polyplexes, treated in the same manner as the respective nanoparticle samples. The following formula was used to calculate encapsulation efficiency after background subtraction of each sample:

$$EE(\%) = 100\% - \frac{mean\ emission_{untreated\ control}}{mean\ emission_{treated\ sample}}\ x\ 100\%$$

2.8. Agarose gel shift assay

A 1.5% (*w*/*v*) agarose gel for Cas9 mRNA / sgRNA polyplexes was prepared by heating up agarose (Agarose BioReagent, Sigma-Aldrich, Merck, Darmstadt) in TBE buffer (18.0 g of tris(hydroxymethyl) aminomethane, 5.5 g of boric acid, 0.002 M disodium ethylenediaminetetraacetic acid (EDTA) at pH 8, in 1 L of water). After cooling down to about 50 °C, 1× GelRed™ (Biotium, Hayward, CA, USA) was added. The agarose solution was casted into an electrophoresis unit and cooled down for gelification. Polyplexes and LNP were formulated as described in the section 2.3 "polyplex formation" and 2.4 "LNP formation", respectively. 3 μL of loading buffer (6×; prepared from 6 mL of glycerol, 1.2 mL of 0.5 M EDTA, 2.8 mL of H_2O, 0.02 g of bromophenol blue) was added to 15 μL of the polyplex solution. Samples were loaded to the pockets of the gel and electrophoresis was performed at 120 V for 70 min in TBE buffer. Free Luc mRNA or a combination of Cas9 mRNA and sgRNA (weight ratio 1:1) diluted in 15 μL HBG to a total RNA concentration of 12,5 g/mL were used as control. Control groups for the evaluation of nanoparticles after incubation in full fetal bovine serum (FBS) were either 15 μL pure FBS, free RNA in 15 μL FBS or free RNA in 15 μL HBG buffer.

2.9. Cell culture

Hepa 1–6 *Pcsk9*^{tdTomato} (a Hepa 1–6 cell line stably expressing tdTomato in the 3'UTR of the *Pcsk*9 gene, generated by HDR-mediated insertion of the 2 A-tdTomato-pA cassette post Cas9-induced double strand break in exon 12 of *Pcsk9*) [60], HeLa mCherry-DMD_{Ex23} (stably expressing an artificial mCherry construct, interrupted by a dystrophin exon 23 sequence, derived from the murine Duchenne muscular dystrophy (DMD) *mdx* model) [61], CT26 eGFP-Luc (stably expressing the green fluorescent protein/luciferase (eGFP-Luc) fusion gene) [50], and HeLa GFPd2 (stably expressing destabilized eGFP) [50] were cultured in Dulbecco'Ss modified Eagles's medium (DMEM)-low glucose (1 g L^{-1} glucose) supplemented with 10% (*v*/v) fetal bovine serum (FBS), 4 mM of stable glutamine, 100 U mL^{-1} of penicillin, and 100 μg mL^{-1} of streptomycin. The cells were cultured at 37 °C and 5% CO2 in an incubator with a relative humidity of 95%.

2.10. Genome editing reporter cell lines

2.10.1. Pcsk9 knock out

For *Pcsk9* knock out studies, sgPcsk9 which binds and directs the Cas9 protein to the first exon of the Pcsk9 gene was used on the Hepa 1–6 *Pcsk9*^{tdTomato} cell line. Thus, the expression of the tdTomato reporter protein is inactivated by the Cas9 induced destruction of the *Pcsk9* gene. The gene knock out of the *Pcsk9* gene can be quantified by flow cytometry as described as described in section 2.11.

2.10.2. mdx DMD_{Ex23} splicing modification

The positive read-out reporter cell line HeLa mCherry-DMD_{Ex23} was used to test the transfection efficiency of Cas9 mRNA/sgDMD_{Ex23} polyplexes. Cas9 induced cleavage at the 3′ prime end of the artificial *mdx* exon 23 construct triggers alternative mRNA splicing with *mdx* exon 23 skipping and mediates expression of functional mCherry protein. The transfection efficiency can be quantified by the percentage of mCherry positive cells measured by flow cytometry as described in section 2.11.

2.10.3. HDR mediated eGFP to BFP conversion

The homologous directed repair (HDR) efficacy was assessed by the conversion of eGFP to BFP in the HeLa GFPd2 cell line expressing destabilized eGFP. HDR-mediated repair following the Cas9-induced double strand break (DSB) of the DNA can replace the 66th amino acid tyrosine (code: TAC) in eGFP sequence with histidine (code: CAT) [62]. In flow cytometric analysis after treatment with Cas9 mRNA/sgGFP/ssDNA-template polyplexes three cell populations were expected: eGFP positive cells representing non-edited cells; eGFP and BFP negative cells indicating gene knock out by non-homologous end joining (NHEJ) of the DSB and BFP positive and eGFP negative cells suggesting HDR-mediated gene correction.

2.11. In vitro evaluation of cellular gene editing efficiency of Cas9 mRNA/sgRNA containing nanoparticles by flow cytometry

All transfections were performed in triplicate in 96-well plates (Corning® Costar, Sigma-Aldrich, Germany). Hepa 1–6 *Pcsk9*^{tdTomato}, CT26 eGFP-Luc, HeLa GFPd2 and HeLa mCherry-DMD$_{Ex23}$ cells were seeded 24 h prior to transfection (7500 cells/well). On the next day, the medium was replaced with 80 μL of fresh pre-warmed medium containing 10% (*v*/v) FBS. The nanoparticles were prepared as described in sections 2.3 and 2.4 resulting in a total RNA concentration of 12.5 μg mL^{-1} (6.25 μg mL^{-1} Cas9 mRNA and 6.25 μg mL^{-1} sgRNA). Required volumes of nanocarrier solutions were pipetted to the corresponding wells and if needed HBG was added to reach the final volume of 100 μL per well. For testing the efficiency of a further reduced dose nanoparticles were 1:10 (*v*/v) diluted with HBG right before the transfection to ensure precise volumetric dosage. The negative control was represented by 20 μl of HBG. After 24 h of incubation HeLa mCherry-DMD$_{Ex23}$ cells were trypsinized, expanded and incubated for an additional 2 days. All other cell lines were expanded after 48 h and incubated for an additional 3 days. For flow cytometric evaluation, cells were collected and resuspended in PBS solution containing 10% (*v*/v) FBS (FACS buffer). All samples were analyzed by flow cytometry using a CytoFLEX S Flow Cytometer (Beckman Coulter, Brea, CA, USA). Shortly before the measurement, 1 ng μL^{-1} of 4′,6-diamidino-2-phenylindole (DAPI) was added and used to discriminate between viable and dead cells. The cellular fluorescence was assayed by excitation of DAPI at 405 nm and detection of emission at 450 nm. For eGFP to BFP conversion studies DAPI was replaced by 1 ng μL^{-1} propidium iodide (PI). The cellular fluorescence was assayed by excitation of PI at 561 nm and detection of emission at 610 nm. Only isolated viable cells were evaluated. The transfection efficiency on HeLa mCherry-DMD$_{Ex23}$ cells was determined as the percentage of mCherry positive cells. The cellular mCherry expression was assayed by excitation at 561 nm and the detection of emission at 610 nm. The cellular tdTomato expression in Hepa 1–6 *Pcsk9*^{tdTomato} cells was assayed by excitation at 561 nm and the detection of emission at 585 nm. The *Pcsk9* knock out efficiency was determined as the percentage of tdTomato negative cells. The cellular GFP expression in CT26 eGFP-Luc and HeLa GFPd2 was assayed by excitation at 488 nm and the detection of emission at 530 nm. The GFP knock out efficiency was determined as the percentage of GFP negative cells normalized to the control measurements with HBG buffer-treated cells. In eGFP to BFP conversion study the loss of GFP indicated gene knock out mediated NHEJ; BFP expression represented conversion from the GFP reporter protein to BFP by homology-directed repair while GFP expressing cells show non-edited reporter cells. BFP expression was assayed by excitation at 405 nm and the detection of emission at 450 nm. Flow cytometry data were analyzed using FlowJo™ v10.8 flow cytometric analysis software by FlowJo, LLC (Becton, Dickinson and Company, U.S.).

2.12. Incubation of polyplexes in high serum

All transfections were performed in triplicate in 96-well plates (Corning® Costar, Sigma-Aldrich, Germany). HeLa mCherry-DMD$_{Ex23}$ cells were seeded 24 h prior to transfection (7500 cells/well). On the next day, the medium was replaced with 80 μL of fresh pre-warmed medium containing 10% (*v*/v) FBS. The nanoparticles were prepared as described in section 2.3. To assess the efficiency in high serum of LAF containing carriers, the polyplexes were 10–20-fold diluted with 100% FBS. After incubation of the polyplexes for 2 h at 37 °C, volumes resulting in the indicated concentration were added to the corresponding wells. To reach a final volume of 100 μL per well in all experiments, either HBG buffer or FBS were added for HBG diluted and serum incubated particles, respectively. Addition of 20 μL HBG buffer was used as negative control. The cells were incubated for 24 h. Afterwards, the cells were trypsinized, expanded and incubated for additional 2 days. Flow cytometric evaluation and analysis was performed as described in section 2.11.

2.13. Assessment of the relative metabolic activity of cells via MTT assay

Transfections were performed as described in section 2.11. At 24 h post transfection, 10 μL dimethylthiazol (MTT) (5 mg mL-^{1}) were added to each well, reaching a final concentration of 0.5 mg mL^{-1}. The supernatant was removed after incubation at 37 °C for 2 h. The plates were stored at −80 °C for at least 1 h. Afterwards, the purple formazan product was dissolved in 100 μL DMSO. After incubation for 30 min at 37 °C under constant shaking (125 rpm), quantification was done photometrically using a Tecan microplate reader (Spectrafluor Plus, Tecan, Männedorf, Switzerland). Absorbance was measured at wavelength λ = 590 nm with background correction at λ = 630 nm. Experiments were carried out in triplicates. Relative metabolic activity related to control wells (HBG-treated cells) was calculated by the equation:

$$\frac{A_{test}}{A_{control}} x\ 100\%$$

2.14. In vitro DNA cleavage assay

To confirm the specificity of the cleavage of the mCherry reporter gene and the genomic donor splice site downstream the physiological dystrophin exon 23 by the RNP complex formed with sgDMD$_{Ex23}$ compared to no cleavage by RNP complex formed with other sgRNAs *in vitro*, 300 ng of a linearized plasmid or PCR amplicon surrounding the physiological dystrophin exon 23 containing the sgDMD$_{EX23}$ target site was generated. The linear DNA or PCR amplicon was then incubated with the precomplexed RNPs (150 ng of Cas9 protein and 60 ng of sgRNA) for 2 h at 37 °C. The reaction mixture was analyzed by agarose gel electrophoresis (1.5% agarose gel). Because of the asymmetric location of the sgDMD$_{EX23}$-target sequence within the amplicon, successful cleavage by the Cas9/sgRNA complex results in two bands on the agarose gel.

2.15. Splicing modulation assay of Cas9 treated HeLa mCherry-DMD$_{Ex23}$ cells

The reporter cell line HeLa mCherry-DMD$_{Ex23}$ was treated with 1611 polyplexes (N/P 18) containing either Cas9 mRNA/sgDMD$_{Ex23}$ (weight ratio 1:1) or Cas9 mRNA/sgPcsk9 (weight ratio 1:1), resulting in concentrations of 10 nM sgRNA. After three days total RNA was isolated from cells using RNASolv (VWR International GmbH, Darmstadt, Germany) according to the manufacturer's protocol. The cDNA synthesis was carried out using the qScript cDNA synthesis kit (Quantabio, Beverly. Massachusetts, USA), utilizing 400 ng of RNA following the manufacturer's protocol. For the amplification of the exon skipping region, a nested PCR was conducted with 150 ng of cDNA, employing Taq polymerase (New England Biolabs, Ipswich, Massachusetts, USA). The specific primer sequences used for the first amplification step were mCherry-DMDex23_SpliSwi_fwd (5'-GGAGGATAACATGGCCATCA-3′) and mCherry-DMDex23_SpliSwi_rev (5'-GTCCTTCAGCTTCAGCCTCT-3′). The PCR conditions used were as follows: initial denaturation (94 °C, 30 s), 30 cycles (94 °C, 30 s / 60 °C, 1 min / 68 °C, 1 min), final extension (68 °C, 5 min). The PCR product was purified using the PCR purification kit from Qiagen (Hilden, Germany) following the manufacturer's protocol. To selectively enrich the splicing product leading to functional mCherry expression, 1 μg of the purified PCR amplicon was subjected to an overnight digestion with 2 units of *Nde* I. The restriction enzyme was removed by adding 1.25 μL of 10% sodium dodecyl sulfate (SDS, *w/v*) (resulting in 0.2% SDS) into the reaction solution and incubating for 10 min at 65 °C. The removal of SDS and the restriction enzyme was accomplished by purifying the digested DNA using the PCR purification kit (Qiagen, Hilden, Germany) in accordance with the manufacturer's protocol. For the subsequent second amplification of the nested PCR

300 ng of the digested and purified DNA as template were used. The PCR was carried out with the primers mCherry-DMD$_{Ex23}$ SpliSwi nested_fwd (5'-GGAGTTCATGCGCTTCAAGG-3′) and mCherry-DMD$_{Ex23}$ SpliSwi nested_rev (5'-GCCGTCCTCGAAGTTCATCA-3′) under the following conditions: initial denaturation (94 °C, 30 s), 30 cycles (94 °C, 30 s / 55 °C, 1 min / 68 °C, 1 min), final extension (68 °C, 5 min). The PCR product obtained from nested PCR was subjected to analysis on a GelRed® (Biotium, Hayward, CA, USA) containing 1% agarose gel in 1× TBE buffer. Electrophoresis was conducted for 1.5 h at 100 V, and the gel was analyzed using the Dark Hood DH-40 (biostep, Burkhardtsdorf, Germany) along with the biostep argusX1 software. The specific target band, indicating the presence of the DNA sequence with skipped dystrophin exon 23 (~280 base pairs (bp)) was excised from the gel. The isolated DNA was purified using the QIAquick® Gel Extraction Kit (Qiagen, Hilden, Germany). For sequence determination, the purified DNA fragments were sequenced (Sanger) by Eurofins GATC Biotech (Konstanz, Germany) using mCherry-DMD$_{Ex23}$ SpliSwi nested_fwd (5'-GGAGTTCATGCGCTTCAAGG-3′) and mCherry-DMD$_{EX23}$ SpliSwi nested_rev (5'-GCCGTCCTCGAAGTTCATCA-3′) primers at a concentration of 10 ng μL^{-1}.

2.16. Confocal laser scan microscopy (CLSM) of Cas9 treated HeLa mCherry-DMD$_{Ex23}$ cells

Transfections of HeLa mCherry-DMD$_{Ex23}$ cells were performed as described above. Cells treated with 1611 containing polyplexes containing either Cas9 mRNA and sgDMD$_{ex23}$ (weight ratio 1:1) or Cas9 mRNA and sgPcsk9 (weight ratio 1:1) resulting in a concentration of 10 nM sgRNA in 96-well plates (Corning® Costar, Sigma-Aldrich, Germany). After 48 h of treatment cells were collected and 20,000 cells were seeded into 8 well-Ibidi μ-slides (Ibidi, Planegg/Martinsried, Germany) in a total volume of 300 μL medium per well. Cells were incubated at 37 °C and 5% CO_2 for 24 h. The next day, cells were washed twice with 300 μL pre-warmed PBS before fixation with 4% paraformaldehyde in PBS for 40 min at RT. The wells were washed again twice with PBS. The cytoskeleton was stained overnight under light exclusion at 4 °C with rhodamin-phalloidin (4 μg mL^{-1} in 300 μL PBS). The cell nuclei were stained with DAPI (2 μg mL^{-1} in 300 μL PBS) for 20 min under light exclusion at RT. The staining solution was removed and 300 μL of PBS was added. The images were recorded using a Leica TCS SP8 SMD confocal laser scanning microscope (CLSM) equipped with an HC PL APO 63 × 1.4 objective (Germany). DAPI and mCherry emission was recorded at 460 nm and 610 nm, respectively. All images were processed using the LAS X software from Leica.

2.17. In vivo studies using Cas9 mRNA / sgDMDEx23 polyplexes and LNPs

In vivo experiments were performed according to the guidelines of the German Animal Welfare Act and were approved by the animal experiments ethical committee of the Government of Upper Bavaria (accreditation number Gz. ROB-55.2–2532.Vet_02–19-19). The study utilized 6-weeks-old female BALB/c mice from Janvier, Le Genest-Saint-Isle, France. Mice were randomly divided into groups of four ($n = 4$ for all formulations) and were housed in isolated ventilated cages under specific pathogen-free conditions with a 12 h day/night interval, and food and water *ad libitum*. Weight and general well-being were monitored continuously. For testing the effect of Cas9 mRNA/sgDMD$_{Ex23}$ formulations *in vivo* on the physiological dystrophin gene, nanocarrier formulations were prepared as described above right before intravenous or intramuscular injection (Cas9 mRNA and sgDMD$_{Ex23}$ at weight ratio 1:1). For systemic application, 150 μL carrier solution containing either 3 μg total RNA in 1762 polyplexes, 1621 LNP and SM-102 LNP or 10 μg total RNA in 1611 polyplexes was intravenously injected into the tail vein at three timepoints (day 0, day 2, day 7). Local administration was performed after subcutaneous treatment with Carprofen at a dose of 5 mg/kg. Single or triple applications (day 0, day 3, day 14) were tested by the injection of 50 μL carrier solution containing either 3 μg total RNA in 1762 polyplexes, 1621 LNP and SM-102 LNP or 10 μg total RNA in 1611 polyplexes into the left musculus biceps femoris. Seven days after the last injection, mice were euthanized and the brain, heart, spleen and musculus biceps femoris (injected left and contralateral right muscle) were harvested. For stabilization of the mRNA, the organs were incubated in RNAlater solution (Thermo Fisher Scientific, Waltham, MA) overnight at 4 °C and stored at −20 °C. Each organ was manually homogenized in liquid nitrogen using mortar and pestle.

2.18. Splicing modulation by Cas9/sgRNA in vivo on mRNA level

The mRNA was isolated for the evaluation of splicing-modulation in the physiological dystrophin gene using the peqGOLD Total RNA Kit (VWR International GmbH, Darmstadt, Germany) according to manufacturer's protocol. 400 ng of the RNA was used to generate cDNA using the total RNA Kit qScript™ cDNA SuperMix (Quanta Biosciences, Gaithersburg, MD, USA) according to manufacturer's protocol. To amplify the region of the exon 23 skipping, 1–5 μL of the cDNA solution were used to perform a PCR using *Taq*^{R} polymerase (New England Biolabs, Ipswich, Massachussets, USA) and the primers amplifying dystrophin-Ex20–26. Following PCR primers and conditions were used: DMD_Ex20–26 fwd (5'-CAGAATTCTGCCAATTGCTGAG-3′) [63]; DMD_Ex24/25 rev (5'-TCACCAACTAAAAGTCTGCATTG-3′) [64]; initial denaturation (94 °C, 30 s), 30 cycles (94 °C, 30 s / 55 °C, 1 min / 68 °C, 1 min), final extension (68 °C, 5 min). The PCR products were purified using the PCR purification kit (Qiagen, Germany). 50 ng of the purified PCR product was used to perform a second PCR with One *Taq*^{R} DNA polymerase and the primers DMD_Ex20/21 fwd (5'-AAAATTTGTAAGGATGAAGTCAAC-3′), DMD_Ex20–24 rev (5'-CAGCCATCCATTTCTGTAAGG-3′). Following PCR conditions were used: initial denaturation (94 °C, 30 s), 30 cycles (94 °C, 30 s / 57 °C, 1 min / 68 °C, 1 min), final extension (68 °C, 5 min).

After performing agarose gel electrophoresis (2% agarose gel; 100 V; 2 h), the PCR products were subjected to band intensity analysis using ImageJ software. The additional bands observed were quantified and compared to the 586 bp full-length dystrophin exon 20–24 sequence. To confirm the exon 23 skipping event in Cas9 mRNA/sgDMD$_{Ex23}$ treated mice, bands of animal #1 treated with LNP 1621 were purified by gel extraction using QIAquick® Gel Extraction Kit (Qiagen, Hilden, Germany). Sanger sequencing of the purified sequences was performed by Eurofins GATC Biotech (Konstanz, Germany) with primers DMD_Ex20/21 fwd and DMD_Ex20–24 rev [65] at a concentration of 20 ng μL^{-1}.

2.19. Genome editing by Cas9/sgRNA in vivo at genomic level

Genomic DNA was isolated for the evaluation of gene editing in the physiological dystrophin gene, using the QIAMP DNA Mini Kit (Qiagen, Hilden, Germany) according to manufacturer's protocol. To amplify the region surrounding the targeted sequence downstream of the exon 23, 100 ng of the DNA solution was used to perform a PCR using *Taq*^{R} polymerase (New England Biolabs, Ipswich, Massachussets, USA). Following PCR primers and conditions were used: DMD genomic fwd (5"-AAACTTCTGTGATGTGAGGACA-3'); DMD genomic rev (5'-ACAAATGGCCAACTATGAGAAAC-3"); initial denaturation (94 °C, 30 s), 30 cycles (94 °C, 30 s / 58 °C, 1 min / 68 °C, 1 min), final extension (68 °C, 5 min). The PCR products were purified using the PCR purification kit (Qiagen, Germany). Sanger sequencing of the purified sequences was performed by Eurofins GATC Biotech (Konstanz, Germany) with primers DMD genomic sequencing fwd (5'-GAAACTCATCAAATATGCGTGTTAGTG-3′) and DMD genomic sequencing rev (5'-GGCAAGTTGCAATCCTTTGA-3′) at a concentration of 20 ng μL^{-1}. Sanger sequencing data was evaluated by the TIDE web tool (https://tide.nki.nl/) applying an indel size range of 25 and default settings for decomposition and alignment windows [66,67]. R^2 values above 0.9

assured the reliability of the model for the analysis of the *in vivo* experiments.

2.20. Statistical analysis

Data were presented as arithmetic mean ± standard deviation (SD) out of at least triplicates, if not otherwise stated. Unpaired Student's two-tailed *t*-test with Welch's correction was performed using GraphPad Prism™ 10 to analyze statistical significances. Significance levels were indicated with symbols: ns $p > 0.05$; *$p \leq 0.05$; **$p \leq 0.01$; ***$p \leq 0.001$; ****$p \leq 0.0001$.

3. Results and discussion

3.1. LAF-Stp carriers for Cas9 mRNA/sgRNA delivery

Scheme 1 displays the design of nucleic acid carriers applied in the current study. As described in [52], polar cationizable succinoyl tetraethylene pentamine (Stp) units [68,69] were combined with a dynamic lipophilic domain featuring a central tertiary amine positioned between their hydrocarbon chains. Branching lysines were utilized to covalently connect the novel moieties to different positions of the polar Stp units (Scheme 1A). These lipo amino fatty acid (LAF) units introduce a pH-dependent switch of polarity to the hydrophobic moieties. As a result of this combination, the dual pH-responsive carriers and the corresponding nucleic acid nanoparticles can behave like molecular chameleons in their microenvironment [52]. Their water solubility and

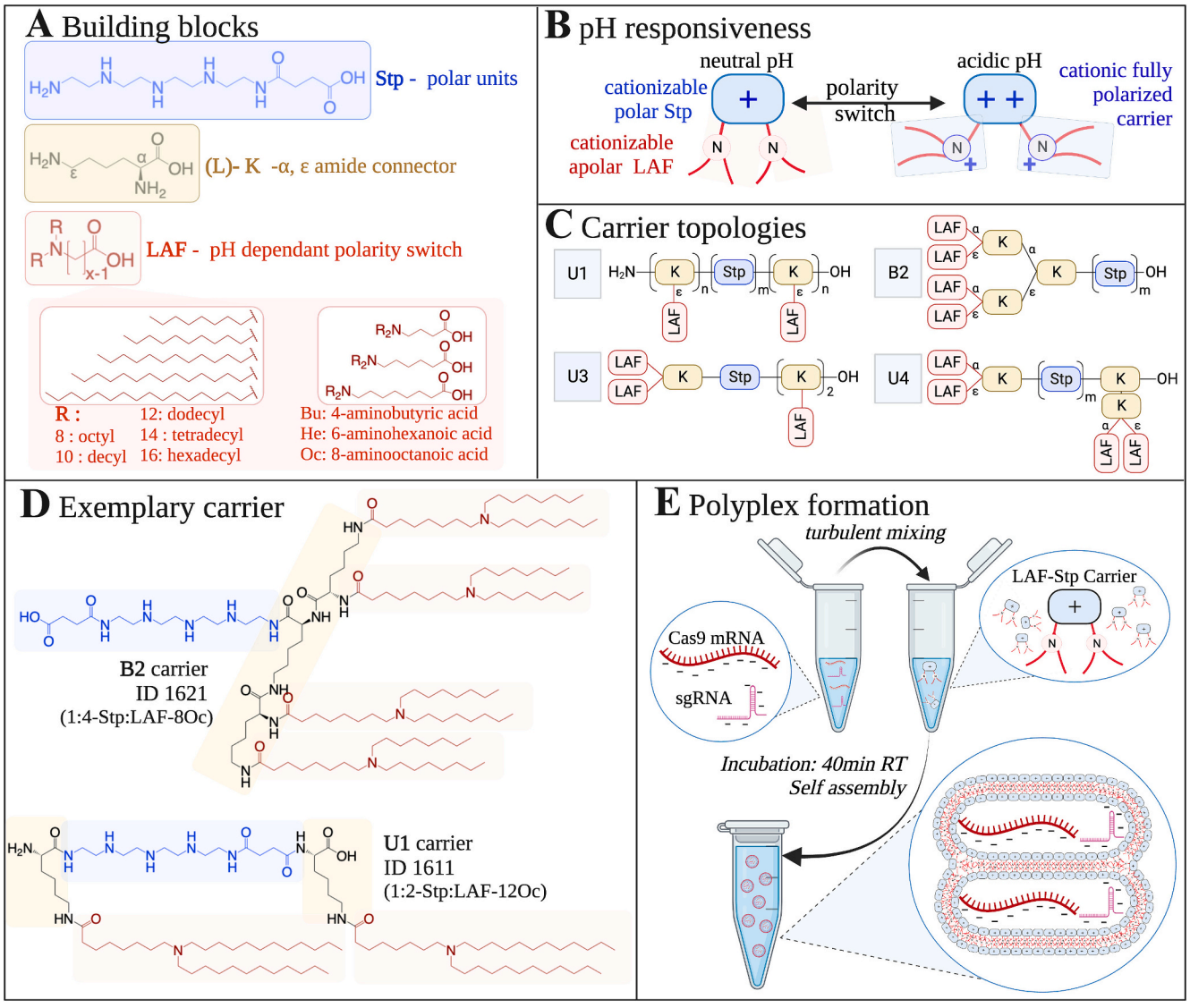

Scheme 1. Lipo amino fatty acid (LAF) – succinoyl tetraethylene pentamine (Stp) carriers as cationizable carriers for polyplex formulation. (A) Building blocks used for the synthesis of LAF-Stp carriers for Cas9 mRNA/sgRNA delivery: Polar Stp (blue) units are connected *via* lysines (yellow) to different LAFs (red). **(B)** pH dependent polarity switch of apolar LAF unit at neutral pH to protonated polar unit at acidic pH **(C)** Chemical motif of four leading LAF-Stp carrier topologies **(D)** Exemplary chemical structures shown for B2 carrier ID# 1621 (8Oc) and U1 carrier ID# 1611 (12Oc). Stp, succinoyl tetraethylene pentamine; (L)-K, lysine; LAF, lipo amino fatty acid. Nomenclature of LAFs: The number (8, 10, 12, 14, and 16) represents the number of C-atoms of the terminal alkyl chains, and the two letters express the ω-amino fatty acid ("Oc", 8-aminooctanoic acid; "He", 6-aminohexanoic acid; "Bu", 4-aminobutanoic acid). For bundles, m = 1, 2; for U-shapes, m = 1, 2 and *n* = 1, 2 (U1). Individual carriers were designated a 4-digit ID number. **(E)** Schematic illustration of polyplex preparation. LAF-Stp carrier and RNA, consisting of Cas9 mRNA and sgRNA (weight ratio, 1:1) are diluted in equal volumes HBG buffer. After combining of both solutions by turbulent mixing and incubation for 40 min at room temperature, polyplexes formed *via* self-assembly.

insolubility switches depending on their protonation (Scheme 1B). When the tertiary amines become protonated within the endosomal environment, aqueous solubility of carriers strongly increases (about 100-fold), reducing hydrophobic interactions and stability of the nanoparticles. All these factors, along with the increased ability of the amphiphilic carriers in protonated stage to disrupt membranes, is assumed to be beneficial for facilitating transmembrane transport and efficient cargo release at the intended intracellular site of action. A library of sequence defined carriers with different topologies was generated by standard Fmoc solid phase assisted peptide synthesis (SPPS). The arrangements of the LAF and Stp units resulted in U-shaped and bundle-shaped topologies with apolar LAF units on both, C- and N-terminus or only the N-terminal side of the Stp, respectively (Scheme 1C). The LAF unit itself was synthesized by reductive amination of different amino fatty acids with fatty aldehydes of numerous lengths. By varying the chain length of both the amino fatty acid and the fatty aldehydes, the position of the tertiary amine within the LAF building block is shifted. Our previous studies revealed that the resulting different LAF types impact both the physicochemical properties and the activity of the corresponding nucleic acid nanoparticles [52,54]. In the LAF nomenclature provided in Scheme 1A, the carbon chain lengths of the terminal alkyl chains are denoted by numerical values (8, 10, 12, 14, 16), and the amino fatty acids within the LAF building block are represented by two-letter abbreviations (Bu, He, Oc). Individual carriers were designated a 4-digit ID number. In total, 20 different LAF-Stp carriers were assessed in the study; **Table S3** provides an overview over the compound library. Exemplary chemical structures of lead carrier 1621 (B2–1:4-Stp:LAF-8Oc) and 1611 (U1–1:2-Stp:LAF-12Oc) are shown in Scheme 1D.

Formulation of Cas9 mRNA and sgRNA with LAF-Stp carrier into Cas9 polyplexes (Scheme 1E) was carried out by turbulent mixing of equal volumes of nucleic acid (Cas9 mRNA and sgRNA at fixed weight ratio 1:1) and LAF carrier solutions in HBG buffer (20 mM HEPES, 5% glucose; pH 7.4). The choice of a 1:1 weight ratio for Cas9 mRNA / sgRNA which presents a high molar excess of sgRNA was based on preliminary testing (**Fig. S1**) and literature precedents [43,70], with the rational that the sgRNA needs to persist in the cytoplasm until Cas9 protein is translated and the RNP is assembled.

After 40 min incubation at room temperature (RT) self-assembly of polyplexes occurred by electrostatic and hydrophobic interactions of nucleic acids and LAF carrier. The N/P ratio calculation corresponds to the molar ratio of amines to the negatively charged phosphates of the nucleic acid cargo (sum of phosphates of Cas9 mRNA and sgRNA). All protonable secondary, tertiary, and terminal amines of the LAF-Stp carrier structure (**Table S3**) were considered for the N/P calculation, irrespective of their actual far lower protonation.

In the following we evaluated the formulated Cas9 polyplexes in terms of their size, polydispersity, surface charge, and nucleic acid compaction/encapsulation (Fig. 1A,B). According to previous findings for Luc mRNA polyplexes [52] we herein focused on four promising LAF carrier topologies, namely U1; U3; U4 with LAF-12Oc and B2 with LAF-8Oc at different Stp/LAF ratios. The physicochemical characterization of Cas9 polyplexes with N/P ratios 12, 18 and 24 was evaluated *via* DLS

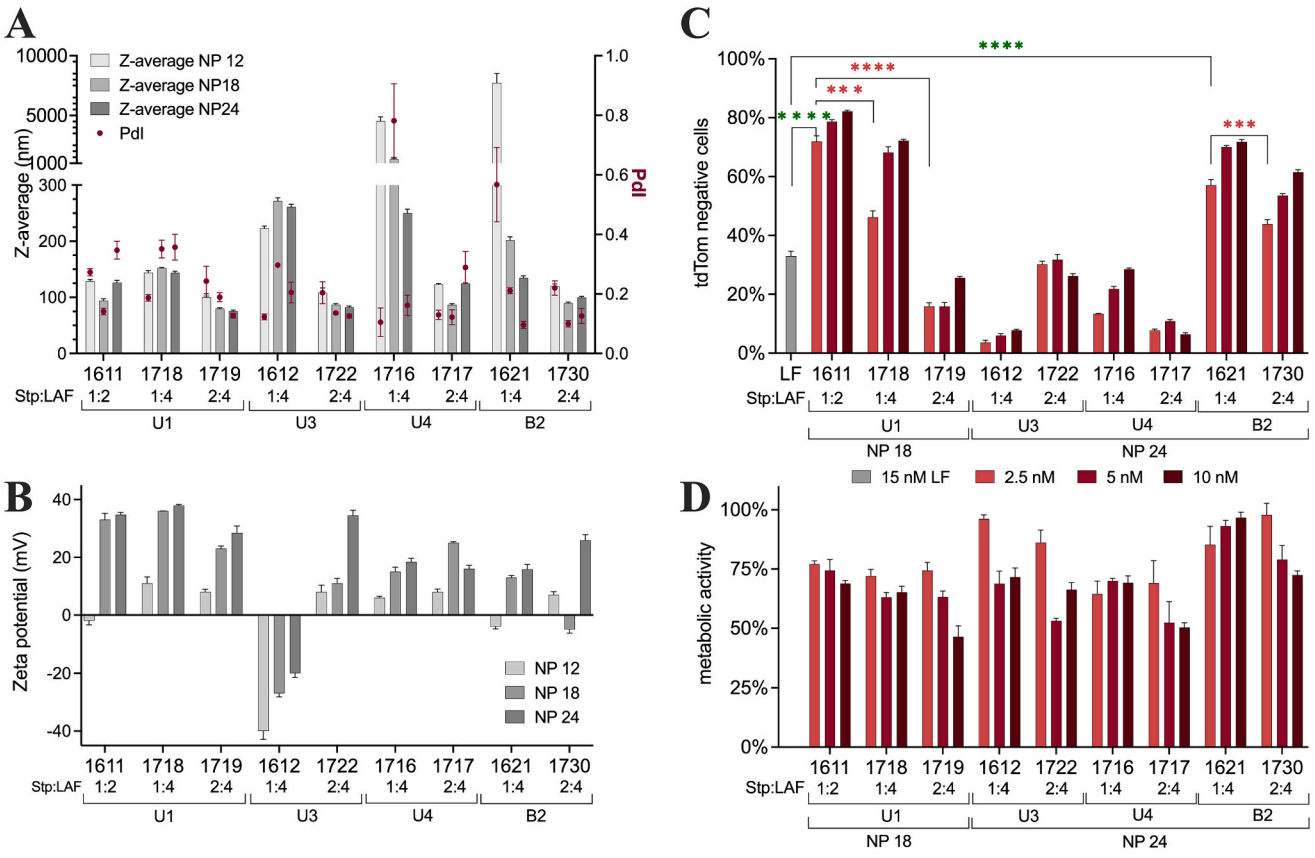

Fig. 1. Physicochemical and biological evaluation of LAF-Stp polyplexes for Cas9 mRNA/sgRNA co-delivery. (A) DLS and **(B)** ELS measurements of Cas9 polyplexes containing Cas9 mRNA and sgPcsk9 at weight ratio 1:1, formed with LAF-Stp carriers (specified by carrier ID number) at indicated N/P ratios and a total RNA concentration of 12.5 μg mL^{-1} ($n = 3$, mean ± SD). **(C)** *In vitro Pcsk9* gene knockout efficiency by Cas9 polyplexes formed with LAF-Stp carriers at optimal N/P ratios. Hepa 1–6 *Pcsk9*^{tdTomato} cells were treated with Cas9 polyplexes at concentrations of 2.5 nM sgPcsk9, 5 nM sgPcsk9 and 10 nM sgPcsk9. Lipofectamine™ Messenger MAX™ lipoplexes (LF) were formed with Cas9 mRNA and sgPcsk9 according to manufacturer's protocol and transfected resulting in a concentration of 15 nM sgPcsk9 in 96-well plates. Gene knockout efficiency was determined by the percentage of tdTomato negative cells 5 days post treatment (n = 3, mean ± SD). **(D)** Metabolic activity of transfected Hepa 1–6 *Pcsk9*^{tdTomato} cells in relation to HBG buffer treated control cells determined *via* MTT assay at 24 h after transfection (n = 3, mean ± SD). Statistical significance levels: ns-not significant $p > 0.05$; *$p \leq 0.05$; **$p \leq 0.01$; ***$p \leq 0.001$; ****$p \leq 0.0001$.

and ELS (Fig. 1A,B; **Table S4**).

Topology independent, all LAF-Stp carriers with two Stp resulted in smaller particles (≈75–125 nm) with higher zeta potential (+ 5–35 mV) than their analogs with only one Stp (exception for B2–2:4; 1730 at N/P 18 (−5.4 mV)). In general, all LAF carrier of the 1 Stp series required higher N/P ratios than those with 2 Stp units for stable polyplex formation. Probably the flexibility of two Stp units led to better electrostatic interactions between cargo and carrier and thereby providing more stability than LAF carriers with a lower Stp/LAF ratio. For the most part, a Stp/LAF ratio of 1:4 was more challenging for nanoparticle formation which might be caused by the steric bulkiness of the LAF building blocks. In U1 carriers, in contrast to the other topologies, where LAF units are linked to the alpha and epsilon amines of lysines, there is maximally one LAF linked per lysine. This seems to result in a better distribution of the sterically demanding LAF within the carrier. Hence, the carrier 1718 (U1–1:4) is the only tested carrier with a Stp/LAF ratio 1:4 able to form small and positively charged Cas9 polyplexes (144–152 nm; + 11–38 mV) at any tested N/P ratios. In the case of 8Oc bundle, B2–1:4 (1621), only Cas9 polyplexes with at N/P ratio ≥ 18 were able to form positively charged particles of acceptable size and PdI whereas, B2–2:4 carrier (1730), obtained stable particles at all tested N/P ratios. Relatively balanced Stp/LAF ratio (*i.e.*, 1:2 or 2:4) and the additional Stp unit might be beneficial here as well. Similar tendencies were observed for U3 and U4–shaped structures. These findings were supported by an agarose gel shift assay showing complete binding of both Cas9 mRNA and sgRNA by all carriers but the negatively charged polyplexes formed with 1612 (**Fig. S2**). Overall, the U1 topology seemed to be most promising in terms of polyplex formation. At any tested N/P ratio, U1 carriers resulted in small Cas9 polyplexes showing no positive effect for increasing the N/P ratio from 18 to 24. For most other LAF-Stp carriers, however, a N/P ratio of 18 resulted in increased polydispersity and a tendency to aggregation indicating to be close to the critical minimal carrier concentration needed for stable particle formation. Rising the N/P ratio to 24, however, led to a more homogenous particle formation. Furthermore, analogues of 1611 (U1–1:2) and 1621 (B2–1:4) with different LAF were evaluated (**Table S4; Fig. S3**). For U1-shaped structures only a LAF with longer terminal alkyl chains (tetradecyl, hexadecyl) showed a slight increase in particle size. Nevertheless, all LAF were able to form positively charged Cas9 polyplexes with a size below 150 nm. B2-shaped carrier with longer LAF (12Oc, 14He; 16Bu) resulted in increased polydispersity and aggregation, despite the high N/P ratio 24. Shorter LAF on the other hand formed monodisperse particles with acceptable size.

The ability of LAF-Stp carriers to co-deliver Cas9 mRNA and sgRNA and induce specific *Pcsk9* gene knock out was evaluated in a Hepa 1–6 cell line, namely Hepa 1–6 *Pcsk9*^{tdTomato}, stably expressing tdTomato from the *Pcsk9* gene (Fig. 1C,D). The sgPcsk9 binds and directs the Cas9 protein to the first exon of the *Pcsk9* gene thus the expression of the tdTomato reporter protein is inactivated by the Cas9 induced destruction of the *Pcsk9* open reading frame. The gene knock out of the *Pcsk9* gene was quantified by flow cytometry. The metabolic activity of cells upon transfection was determined *via* MTT assay to assess the tolerability of the carriers. Cas9 polyplexes formed with LAF carriers at N/P ratio 12, 18, and 24 were transfected at 2.5 nM–10 nM sgPcsk9 (≈ 16 ng–66 ng total RNA, weight ratio 1:1 for Cas9 mRNA and sgPcsk9) in Hepa 1–6 *Pcsk9*^{tdTomato} and compared to gold standard lipofection of 100 ng total RNA (≈ 15 nM sgPcsk9) with Lipofectamine™ Messenger MAX™. Overall U1 and B2 shaped carrier outperformed the other U shape topologies. At 6-fold lower dose, U1 and B2 Carriers with only one Stp showed significantly higher knock out than the Lipofectamine control. In contrast to their superiority for nucleic acid compaction and particle formation, carriers with a Stp/LAF ratio of 2:4 showed significantly reduced efficiency compared to their analogs containing only one Stp. This indicates that the right balance in between nucleic acid compaction and cargo release at its site of action is crucial for the transfection efficiency of Cas9 polyplexes. It is interesting to note that at lower N/P ratios, knock-out events showed a strong correlation with the transfected dose, whereas editing events after transfection with nanoparticles at N/P 24 were nearly dose independent (**Fig. S2**). This demonstrates that the transfection efficiency is mainly dependent on the amount of carrier reaching each cell, rather than the cargo concentration. We assume that, upon acidification in the endosomes, a critical minimal amount of LAF units is needed to enable endosomal escape and release of the nucleic acid cargo. The pronounced effect for carriers with an Stp/LAF ratio of 2:4 supports this hypothesis. The transfection efficiency of LAF-Stp containing Cas9 polyplexes was also confirmed by GFP knock out on CT26 eGFP-Luc and HeLa GFPd2 cells (Fig. 2), however, variations in efficacy were observed. The different transfection efficiencies across diverse cell types have been frequently observed in our own and other studies for various nucleic acid cargos, based on differing cell entry routes, intracellular trafficking and endosomal escape [36,71]. Furthermore, effects of LAF side chain variations (Nitrogen Catwalk) in the best performing topologies (U1–1:2; B2–1:4) on gene editing efficiencies in different cell types were assessed (**Fig. S4, Fig. S5**). Gene editing efficiency upon transfection of Cas9 polyplexes was assessed at further reduced dose (0.5 nM–5 nM sgRNA) and compared to gold standard transfections with 100 ng total RNA (≈ 15 nM sgRNA) Lipofectamine™ Messenger MAX™, or 250 ng total RNA (≈ 38 nM sgRNA) as polyplexes formed with succinylated PEI (succPEI) at weight ratio 4:1, succPEI: total RNA [72]. Longer terminal carbon chains (tetradecyl; hexadecyl) which have already demonstrated negative effects on particle properties, showed almost no gene editing events on any tested cell line. Among the various LAF chain lengths, the initially tested LAF-Stp 1611 (12Oc) demonstrated the highest gene editing events compared to its analogs (**Fig. S4**). Gene editing events were scarce in all cell lines following the transfection with 1746, an U1 analog with LAF 8Oc. On the other hand, for B2 carriers, LAF 12Oc revealed counterproductive effects on both gene editing and polyplex formation, whereas the four shorter LAFs (8Oc, 12Bu, 10Oc, 12He), formed small Cas9 polyplexes demonstrating gene editing efficiency on all tested cell lines (**Fig. S5**). Cell line dependent effects where more pronounced for B2 carriers. Transfection of Hepa and CT26 with B2 carriers containing 8Oc or 10Oc did not hamper the metabolic activity of the cells. Concentrations of only 2.5 nM sgRNA yielded equal to or higher knock out results than those of both positive control groups, despite the manifold higher concentration. In HeLa cells, all B2 carrier containing one of the four shorter LAF (8Oc, 12Bu, 10Oc, 12He) exhibited a very high gene editing efficiency over 50%. Even at lowest tested concentrations of 0.5 nM sgRNA, both positive control groups were outperformed. It is worth noting that structures exhibiting greater transfection effectiveness often display higher toxicity, compared with structures of lower efficiency. It is likely that the mechanisms responsible for effective delivery, such as destabilizing lipid membranes, initiate certain levels of cytotoxicity. Nonetheless, this toxicity can be managed by reducing the concentration. Overall, variations of the LAFs influenced polyplex formation and physicochemical properties (**Table S4, Fig. S3**), transfection potency and toxicity (**Fig. S4**; **Fig. S5**) of corresponding Cas9 polyplexes. Consistent with Thalmayr et al. [52], 12Oc containing 1611 emerged as the most promising among U1-shaped carriers, while for bundles, a shorter LAF not only enhanced nanoparticle formation but also yielded superior results in gene editing. Carrier-1762, which contains the intermediate length LAF (10Oc), demonstrated an improved metabolic activity profile among those tested, without compromising the carrier's effectiveness.

3.2. LAF-Stp carrier 1611 for HDR mediated eGFP to BFP conversion

Having demonstrated that LAF-Stp carriers form potent polyplexes for Cas9 mRNA and sgRNA delivery, enabling gene knockouts through non-homologous end joining (NHEJ), we aimed to broaden its utility by exploring the co-delivery of Cas9 components and a single-stranded DNA (ssDNA) template for facilitating gene knock-ins *via* homology-directed repair (HDR). Firstly, we evaluated whether LAF-Stp carriers

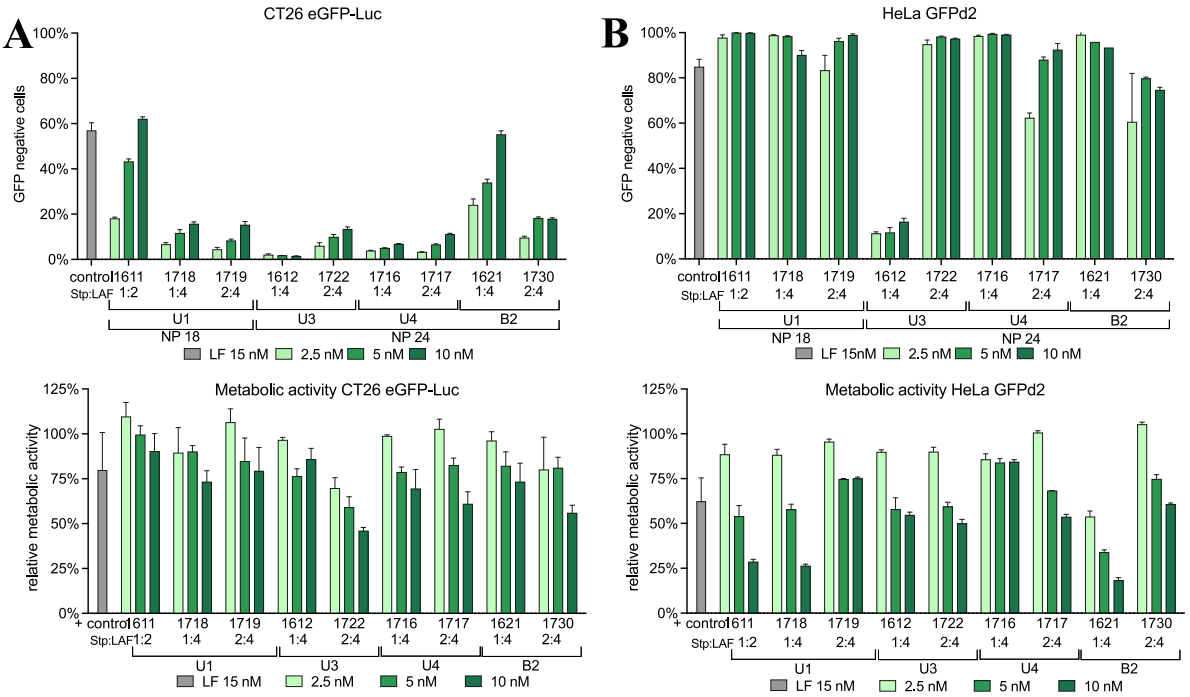

Fig. 2. ***In vitro*** **eGFP knockout efficiency and metabolic activity of different reporter cell lines after treatment with Cas9 polyplexes** containing Cas9 mRNA and sgGFP at weight ratio 1:1, formed with LAF-Stp carriers at optimal N/P ratios**.** Lipofectamine™ Messenger MAX™ lipoplexes (LF) were formed with Cas9 mRNA and sgGFP according to manufacturer's protocol and transfected resulting in a concentration of 15 nM sgGFP in 96-well plates. Gene knockout efficiency was determined by the percentage of GFP negative cells normalized to HBG treated cells, 5 days post treatment. ($n = 3$, mean ± SD) **(A)** top: CT26 eGFP-Luc cells were treated with Cas9 polyplexes at concentrations of 2.5 nM sgGFP, 5 nM sgGFP and 10 nM sgGFP. bottom: Metabolic activity of transfected CT26 eGFP-Luc cells in relation to HBG buffer treated control cells determined *via* MTT assay at 24 h after transfection **(B)** top: HeLa GFPd2 cells were treated with Cas9 polyplexes at concentrations of 2.5 nM sgGFP, 5 nM sgGFP and 10 nM sgGFP. bottom: Metabolic activity of transfected HeLa GFPd2 cells in relation to HBG buffer treated control cells determined *via* MTT assay at 24 h after transfection.

could form stable polyplexes containing both RNA and DNA compounds. Therefore, a small selection of 1-Stp U1 and B2 carriers were tested as polyplexes with mCherry mRNA and GFP pDNA at weight ratio 1:1. The nanoparticles were transfected in different cell lines and mCherry and GFP expression was assessed by flow cytometry (**Fig. S6A—I**). For the physicochemical evaluation, DLS and ELS measurement as well as an agarose gel shift assay were performed (**Fig. S6J, K**). Although the binding of pDNA was incomplete, the carriers, which exhibited robust transfection capabilities for Cas9 mRNA/sgRNA, were also able to effectively co-deliver both mRNA and pDNA into cells yet demonstrating a stronger transfection profile for mRNA. The carrier 1611 was found to be highly effective in co-delivering mRNA and pDNA across all tested cell lines, leading to its selection for the gene knock-in studies through HDR. For this research, a HeLa cell line that expresses a less stable variant of green fluorescent protein (HeLa GFPd2) was utilized [50]. Through HDR-mediated DNA repair, the eGFP gene sequence can potentially be converted into blue fluorescent protein (BFP) gene sequence, and therefore be evaluated by flow cytometry (Fig. 3A,B). All 1611 polyplexes at N/P ratio 18, with Cas9 mRNA plus sgGFP (weight ratio 1:1), with and without a single-stranded DNA template (ssDNA) at three different ratios to the sgRNA, formed small homogeneous particles with positive zeta potential (**Table S5**). These polyplexes were transfected at different concentrations in HeLa GFPd2 cells. As expected, gene knock out efficiency after transfection with Cas9 polyplexes without additional ssDNA template was in line with previous results of transfections in this cell line (**Fig. S4C**) and no BFP positive cells could be detected. Within the tested ratios of sgRNA to ssDNA, ranging from 1:05 to 1:2, we observed that the HDR efficiency increased with higher ratios of ssDNA template, resulting in up to 38% BFP converted cells (Fig. 3C). Interestingly, the overall gene editing efficiency defined by the sum of GFP knock out and BFP converted cells decreased at higher ssDNA ratios. The highest transfected concentrations reached 86%, 82%, 72% and 58% gene edited cells for sgRNA to ssDNA ratios from 1:0 to 1:2, respectively. This suggests that while the RNP's ability to induce double-strand breaks (DSB) is hindered when there are elevated single-stranded DNA (ssDNA) concentrations, the chances of achieving homology-directed repair (HDR) integration are higher when the ssDNA template is in close proximity. To exclude that lower editing efficiencies are triggered by increased carrier concentrations, we tested different sgRNA to ssDNA ratios while keeping the total transfected nucleic acid amount constant (**Fig. S7**). Once more, a decline in general editing effectiveness can be noted with increased template ratios. Instances where 3.9 nM sgRNA were applied with polyplexes lacking ssDNA triggered over 85% GFP knock out, whereas utilizing polyplexes at sgRNA to ssDNA ratios of 1:2 and 1:6 with the same sgRNA concentration yielded total edited cell percentages of only 40% and 21%, respectively (**Fig. S7**). The HDR percentage of total edited cells, however, increased with higher template ratios even though the overall efficiency was reduced (**Fig. S8**).

3.3. Positive read out reporter model for genome editing triggering exon skipping

A reporter cell line HeLa mCherry-DMD$_{Ex23}$, expressing mCherry interrupted by a Duchenne muscular dystrophy (DMD) *dystrophin* exon 23 with nonsense mutation, was recently designed by Lessl et al. [61] (see Fig. 4A). It enabled efficient *in vitro* screening of the antisense activity of phosphorodiamidate morpholino oligomers (PMOs) and their conjugate formulations. The specific PMO(Ex$_{23}$) sequence blocks a splice site of dystrophin pre-mRNA and prompts the skipping of mutated dystrophin exon 23. Such an exon skipping has been therapeutically applied in the well-established murine DMD *mdx* model. Notably, this specific genetic sequence can also trigger exon skipping of the healthy dystrophin in wild-type mice. To ensure the effective use of the same PMO(Ex$_{23}$) sequence in both the *in vitro* reporter system and *in vivo*

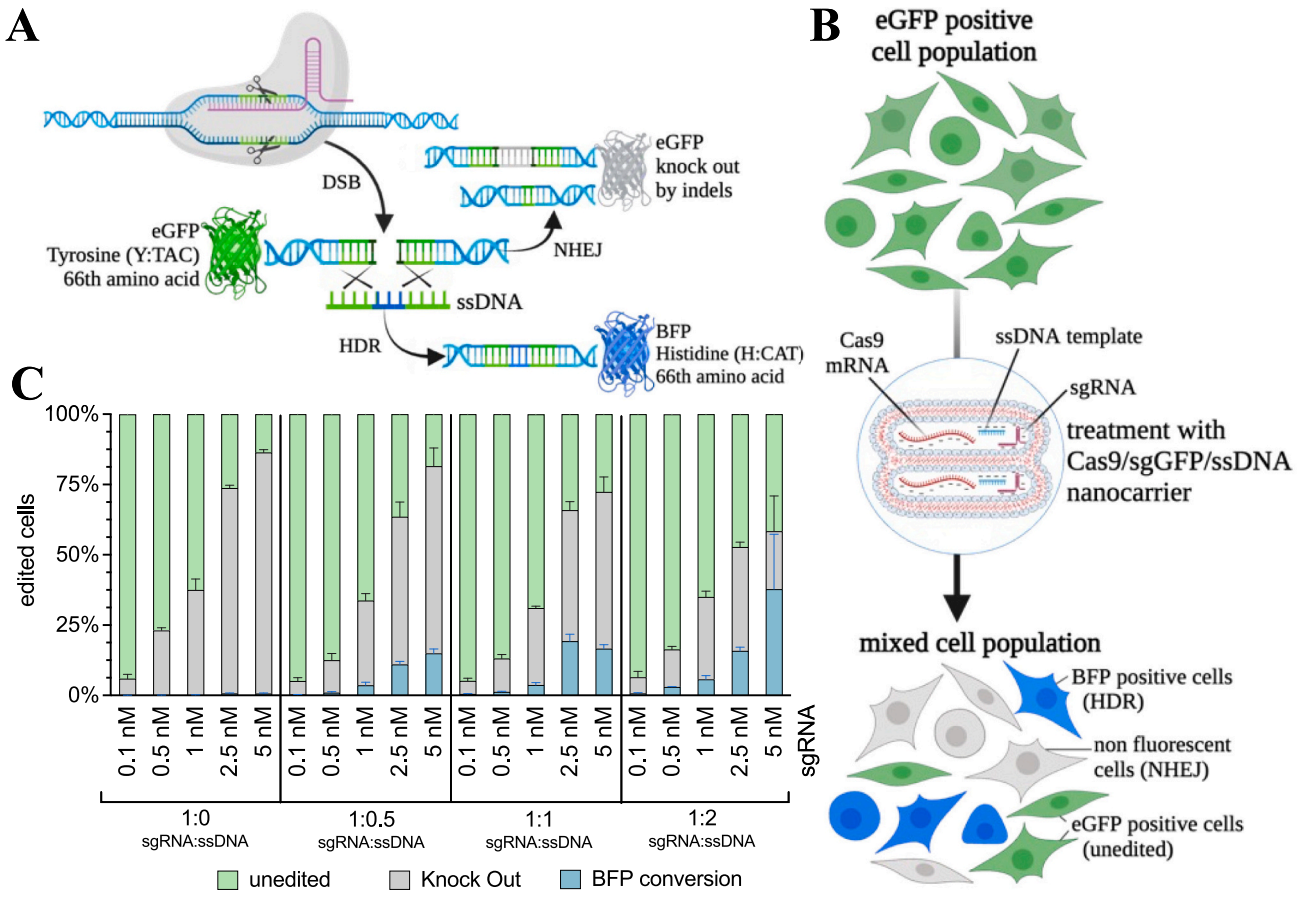

Fig. 3. HDR mediated eGFP to BFP conversion. (A) Schematic illustration of cellular eGFP to BFP conversion after Cas9 induced double strand break (DSB) in the presence of a ssDNA template. Insertion or deletion of bases mediated by non-homologous end joining (NHEJ) pathways lead to eGFP knock out. HDR-mediated DNA repair leads to substitution of tyrosine (TAC), the 66th amino acid, in the eGFP sequence by histidine (CAT). Hereby, eGFP is converted into blue fluorescent protein (BFP). **(B)** Schematic illustration of a population of HeLa GFPd2 cells treated with nanocarriers formed with Cas9 mRNA and sgGFP and a single stranded DNA template (ssDNA). The efficiency of the carriers for gene knock out and HDR mediated conversion to BFP can be evaluated by flow cytometry. **(C)** Editing percentages were evaluated by flow cytometry 5 days after transfection with 1611 polyplexes formed at N/P ratio 18 with Cas9 mRNA and sgGFP (weight ratio 1:1) and a ssDNA template at indicated molar ratios to the sgRNA. Concentrations refer to sgRNA content. ($n = 3$, mean ± SD). (For interpretation of the references to colour in this figure legend, the reader is referred to the web version of this article.)

experiments, the donor splice site of the intron downstream of *mdx* exon 23 was designed based on the physiological donor splice site sequence of dystrophin intron 23. We now selected a sgRNA (sgDMD$_{Ex23}$) [64,73] targeting the same specific donor splice site and evaluated the feasability of a Cas9-based single-cut gene editing approach on this positive read-out reporter model to test the efficiency of Cas9 mRNA/sgDMD$_{Ex23}$ polyplexes. According to reports, precise genetic modification is not necessary for the correction of DMD defects *via* exon skipping. Rather, any indels introduced by NHEJ disrupting a splice donor or acceptor sequence in a mutant exon can lead to exon skipping [73]. By the sgDMD$_{Ex23}$ a double strand break (DSB) in the proximity of the donor splice site of the targeted dystrophin exon 23 is generated. INDELs introduced in the target locus after NHEJ repair lead to the correction of the reporter gene open reading frame (ORF) resulting in observable functional mCherry expression through fluorescence detection (Fig. 4A).

The ORF can be restored by: (i) exon skipping if the INDELs disrupt the splice consensus site of the targeted exon, or (ii) exon reframing if the right number of INDELs is generated in the exonic region [74]. To confirm the specificity of the sgDMD$_{EX23}$ to the target sequence in the reporter construct, we performed an *in vitro* cleavage assay (Fig. 4B). The reporter plasmid DNA construct was linearized and then exposed to ribonucleoprotein complexes (RNPs) containing either sgDMD$_{Ex23}$, sgGFP, or sgPcsk9. Only incubation with the Cas9/sgDMD$_{Ex23}$ complex induced cleavage of the reporter DNA resulting in two bands on the agarose gel (Fig. 4B). The reporter cell line HeLa mCherry-DMD$_{Ex23}$ was treated with 1611 polyplexes (N/P 18) containing either Cas9 mRNA/sgDMD$_{Ex23}$ (weight ratio 1:1) or Cas9 mRNA/sgPcsk9 (weight ratio 1:1). Three days post treatment, total RNA was extracted from treated cells and reverse transcribed into cDNA. The splicing product leading to functional mCherry expression was amplified and analyzed *via* gel electrophoresis. The band resulting from mdx exon 23 skipping (~280 bp) was only detected in cells treated with sgDMD$_{Ex23}$ and exon 23 skipping was confirmed by Sanger sequencing (Fig. 4C). Additionally, the presence of mCherry protein was further determined by confocal laser scanning microscopy (CLSM) images of HeLa mCherry-DMD$_{Ex23}$ cells 72 h after transfection with 1611 polyplexes (N/P 18) containing either Cas9 mRNA and sgDMD$_{Ex23}$ or sgPcsk9 (Fig. 4D). mCherry fluorescence was detectable solely in cells treated with sgDMD$_{Ex23}$. For genomic evaluation of the Cas9 induced edits on the mCherry-DMD$_{Ex23}$ reporter, total genomic DNA was isolated from HeLa mCherry-DMD$_{Ex23}$ cells 2 weeks after treatment with either 1611 (N/P 18) or 1752 (N/P 24) polyplexes containing Cas9 mRNA and either sgPcsk9 or sgDMD$_{Ex23}$ (**Fig. S10**). In groups treated with Cas9 mRNA/sgPcsk9, gel electrophoresis of the PCR products revealed only one band with the expected length (841 bp) of the complete unedited sequence. Additional bands of approximately 450 bp were observed in all groups treated with Cas9

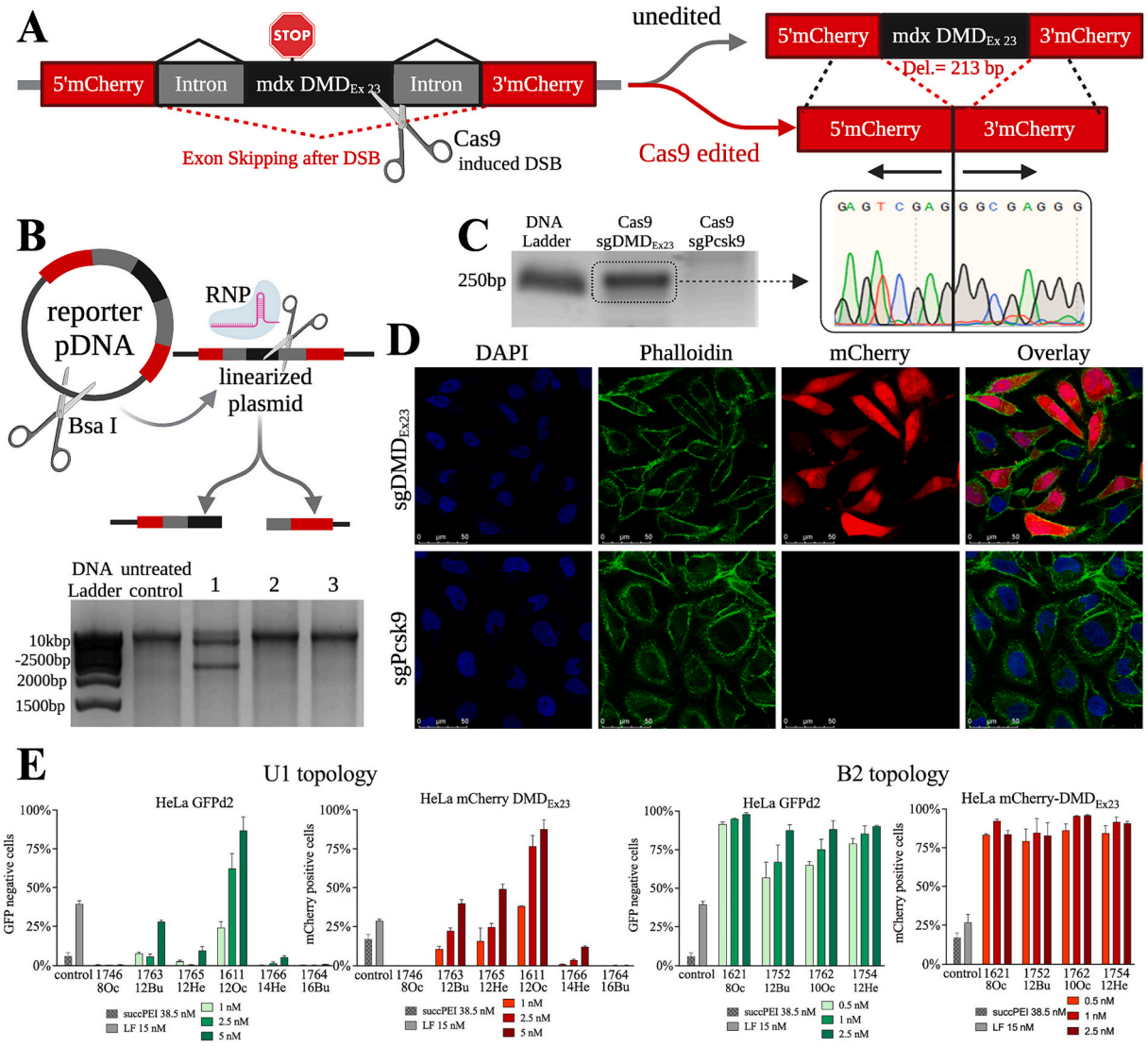

Fig. 4. Positive read-out reporter model for genome editing. Functional mCherry expression is induced in HeLa mCherry-DMDex23 reporter cell line after Cas9 induced DSB. **(A)** Schematic illustration showing the structure of mCherry-DMD$_{Ex23}$ construct and its mechanism in presence or absence of Cas9 induced DSB at the donor splice site downstream the *mdx* exon 23. **(B)** *In vitro* cleavage of the plasmid DNA which was used for the generation of the HeLa mCherry-DMD$_{Ex23}$ cell line after overnight digestion of the plasmid DNA with the restriction enzyme *Bsa*I to linearize the DNA. The linearized DNA was incubated with RNP for 2 h at 37 °C and subsequently analyzed on a 1.5% agarose gel. Untreated linearized plasmid was used as control group; 1: linearized plasmid treated with RNP containing sgDMD$_{Ex23}$; 2: linearized plasmid treated with RNP containing sgGFP; 3: linearized plasmid treated with RNP containing sgPcsk9. **(C)** Detection of *mdx* exon 23 skipping of mCherry-DMD$_{Ex23}$ mRNA by RT-PCR. Total RNA was extracted from cells 3 days after treatment with Cas9 polyplexes formed with LAF 1611 at N/P 18 (10 nM sgDMD$_{Ex23}$ or 10 nM sgPcsk9). The sequence surrounding *mdx* exon23 in mCherry-DMDEx23 was amplified by RT-PCR. The band resulting from *mdx* exon 23 skipping is shown (~280 bp) and exon 23 skipping was confirmed by Sanger sequencing. **(D)** CLSM images of HeLa mCherry-DMD$_{Ex23}$ cells 72 h after transfection with 1611 polyplexes (N/P 18) containing either Cas9 mRNA and sgDMD$_{Ex23}$ (weight ratio 1:1) or Cas9 mRNA and sgPCSK9 (weight ratio 1:1) resulting in a concentration of 10 nM sgRNA. Nuclei were stained with DAPI (blue), cytoskeleton was stained with rhodamine phalloidin (green) and mCherry is shown in red. Scale bar represents 50 µm. RNP: ribonucleoprotein; CLSM: confocal laser scanning microscopy. Complete gels of B) and C) are provided in **Fig. S9**. **(E)** Nitrogen Catwalk of LAF-Stp carriers with U1 topology (left) or B2 topology (right), comparing editing efficiencies in HeLa GFPd2 and HeLa mCherry-DMDex23 reporter cell lines. For details see **Fig. S4** and **Fig. S5**. (For interpretation of the references to colour in this figure legend, the reader is referred to the web version of this article.)

mRNA/sgDMD$_{Ex23}$, indicating large genomic deletions (**Fig. S10A**). Sanger sequencing of the isolated bands confirmed the full sequence of the unedited 841 bp band and a 388 bp long deletion, surrounding the Cas9 cut side, for the shorter band (**Fig. S10D**). The untypical large deletion after Cas9 induced double strand break might be caused by locus specific properties of the artificial construct surrounding the *mdx*-DMD$_{Ex23}$ sequence [75,76]. Nevertheless, the specificity of the reporter for the testing of sgDMD$_{Ex23}$ containing Cas9 formulations was proven by the comparison to sgPcsk9 containing formulations as stated above. Additionally, gene editing results on HeLa mCherry-DMD$_{Ex23}$ cells evaluated by flow cytometry strongly correlate with the GFP knock out data on the HeLa GFPd2 cell line confirming the suitability of this reporter model for library screening (Fig. 4E and **Fig. S4** and **S5**).

3.4. Characterization of top performing polyplexes for in vivo application

While it was evident that 1611 proved to be the optimal carrier for the U-shaped LAF-Stp topology, the trends associated with various B2-shaped carriers were less distinct. Consequently, the subsequent analysis focused on 1611 alongside three promising representatives of B2-shaped carrier candidates, specifically 1621, 1752, and 1762, at a further reduced dosage. As pathways and routes differ between various

cell types, also efficiency ranking of different carriers can be different, as demonstrated in Fig. 5 for Hepa and HeLa. The *Pcsk9* knock out after treatment with a dose range from 0.25 nM to 15 nM sgPcsk9 was evaluated in Hepa 1–6 *Pcsk9*^{tdTomato} cells and compared to Lipofectamine™ Messenger MAX™ lipoplexes, resulting in sgPcsk9 concentrations of 5 nM, 10 nM, and 15 nM as positive control. All LAF-Stp carriers achieved 2–5-fold higher knock out efficiencies than the positive control at corresponding concentrations. Carrier 1611 showed an EC_{50} (defined as the concentration of delivered sgRNA required to provoke 50% gene edited cells) of ~1 nM sgRNA whilst all B2 carriers resulted in $EC_{50} \geq 4.0$ nM sgRNA (Fig. 5A, **Table S6**). Given the previously shown high efficiency of LAF-Stp carriers on HeLa cells, we chose an ultra-low dose range from 50 pM to 2.5 nM sgRNA for the evaluation on HeLa mCherry-DMD_{Ex23}. Interestingly, a strong benefit of the B2 topology could be observed in this cell line resulting in >10-fold lower EC_{50} values (0.1 nM to 0.4 nM $sgDMD_{Ex23}$) compared to the EC_{50} in Hepa 1–6. Gene editing of 1611 polyplexes (EC_{50}: 0.7 nM $sgDMD_{Ex23}$), on the other hand, was comparable to the results on Hepa cells (Fig. 5B). Consistent with prior research, a connection between increased potency and toxicity at elevated doses was evident. Notably, while among all the evaluated carriers only compound 1611 reduced the metabolic activity of Hepa 1–6 cells at higher doses, the metabolic activity of HeLa cells was only reduced by higher doses of the B2 carrier 1621 (**Fig. S11**).

There is a significant disparity between the *in vitro* conditions in cell culture and those in animal models (*in vivo*). Upon intravenous administration of nanoparticles, their interaction with blood components may critically influence on their performance [77,78]. Hence, transfection efficiency was evaluated after pre-incubation of the polyplexes in full (≥ 90% *v*/v) serum at 37 °C for 2 h (Fig. 5C). Notably, despite full serum incubation efficacies of top carriers were not reduced, with sub-nanomolar EC_{50} values of as low as 0.4 nM $sgDMD_{Ex23}$ for carrier 1611 and 0.1 nM $sgDMD_{Ex23}$ for carrier 1762. Consequently, carrier 1611 at N/P 18 and carrier 1762 at N/P 24 emerged as the most suitable candidates for *in vivo* evaluation of U1 and B2 topologies, respectively. Concentrated formulations intended for *in vivo* application underwent testing for their physicochemical properties, demonstrating resistance toward full serum, long-term stability upon storage at 4 °C for up to 127 days, and high transfection efficiency after 14 days storage at 4 °C (**Table S7, Fig. S12, Fig. S13**). Successful delivery of nanocarriers into specific tissues is often facilitated by their surface interactions with distinct serum proteins and subsequent binding to their cognate receptors [13,79] and following productive intracellular routing. Therefore, the transfection efficiency of the nanocarriers was assessed subsequent to dilution of the concentrated formulations in full serum (**Fig. S13**). These results further confirm the feasibility of using these structures for *in vivo* testing.

3.5. In vivo editing of dystrophin gene

Optimized LAF-Stp carriers formulated with mRNA either as polyplexes [52] or as cationizable component in LNPs [54] were found to efficiently deliver luciferase mRNA at low 1–10 μg mRNA/mouse doses upon intravenous application in A/J mice. Combined with the current *in vitro* findings, we selected the promising carriers 1611 and 1762 for polyplex formulation as well as a 1621-based LNP formulation for Cas9 mRNA/sgRNA delivery *in vivo*. Biophysical characterization of 1621 LNP is presented in **Tables S8, S9**; **Fig. S14**. Similar to the polyplexes, the selected LAF-Stp LNP formulations exhibited remarkable long-term stability (storage at 4 °C for 127 days). In contrast to parallel tested gold standard SM-102-containing LNP, they still induced gene editing upon transfection following 14 days of storage at 4 °C (**Fig. S13**).

For Cas9-induced dystrophin gene editing in healthy mice *in vivo*, the same $sgDMD_{Ex23}$ sgRNA sequence can be applied as in the positive readout reporter model described in section 3.3 and originally designed for assessment of splice-switching oligonucleotides by Lessl et al. (**Fig. S9C**). Using PMO(Ex_{23}) conjugates of related sequence-defined xenopeptides, Lessl et al. could demonstrate *in vivo* dystrophin exon 23 skipping in several organs. By Cas9 mediated genomic disruption of the donor splice site, the efficiency of gene editing can be assessed by: (i) examining the genomic sequence in the vicinity of the specific cleavage site, and (ii) analyzing exon skipping at the mRNA level. Genome editing and mRNA splicing modulation after intravenous injection with Cas9 polyplexes and Cas9 LNPs in BALB/c mice is displayed in Fig. 6. During a 7-day period, BALB/c mice were subjected to three intravenous injections, receiving either 1762 polyplexes or 1621 LNPs, both containing 3 μg total RNA (Cas9 mRNA and $sgDMD_{Ex23}$ at a weight ratio of 1:1). Well tolerable 1611 polyplexes contained 10 μg total RNA. Good biocompatibility of all formulations was demonstrated by standard plasma parameters (ALT, alanine transaminase; AST, aspartase aminotransferase; Crea, creatinine; BUN, blood urea nitrogen) and monitoring the body weight of animals (**Fig. S15, S16**). The *ex vivo* assessment of dystrophin genome editing and mRNA exon 23 skipping was performed only with organs exhibiting high dystrophin expression [80], *i.e.* brain, heart, and biceps femoris muscle. We aimed to minimize other factors that might compromise gene editing efficiency *i.e.* chromatin modifications and DNA packaging that can block eukaryotic genome editing [81]. Analysis was performed seven days after final intravenous administration and compared to results of untreated BALB/c mice. Confirmation of the desired exon 23 skipping in the physiological dystrophin mRNA was achieved by representative Sanger sequencing of the RT-PCR products isolated from an agarose gel (Fig. 6C, D). RT-PCR products showed significant exon skipping in various groups (Fig. 6F). The 1621 containing LNP formulation resulted in significantly higher exon 23 skipping rates in heart tissue (5.7% ± 1.1%; mean ± SD) than both polyplex formulations. Splicing modulation in the brain was evident across all examined formulations. Especially, 1762 polyplexes elicited an high exon skipping rate of 13.1% ± 4.4% (mean ± SD) in brain tissue. Both the 1611 polyplex and the LNP 1621 group displayed considerable variability, with certain individual animals exhibiting higher splicing modulation compared to others. Considerable variability was similarly observed in skeletal muscle across all groups. High splicing modulation values of up to 17%, stood in contrast to low levels of other individuals.

Such differences in between the individual groups, tissues and individuals were not observed in the genomic evaluation of the gene sequence surrounding the expected cut site at the dystrophin exon 23. Using the TIDE analysis tool, total gene editing efficiencies of 2.5% - 4.7% were detected in organs of treated animals compared to a background signal of <0.7% in untreated animals (Fig. 6G). Even though significant gene editing values could be detected in most groups the editing values are lower than splicing modulation values in corresponding animals (**Table S11**). On the one hand it remains unclear which exact indel sequence causes a change in the splicing pattern of exon 23, on the other hand possible larger genomic deletions, as shown in the mCherry-DMD_{Ex23} reporter model, would not be detectable by the TIDE analysis tool. The positive control LNP SM-102 mediated comparable genome editing efficiencies as LNP 1621.

The next aim was to investigate genome editing and mRNA splicing modulation after local intramuscular injection with Cas9/sgRNA polyplexes and LNPs. As the i.m. administration of the novel class of carriers had not been studied in previous work, the efficiencies of polyplexes and LNPs were first analyzed by intramuscular application using luciferase reporter mRNA (**Table S10, Fig. S18**). Within the class of mRNA polyplexes, all displayed a very high i.m. luciferase expression around 10^8–10^9 RLU/g muscle at 6 h post-injection; the bundle B2 carrier 1762 exhibited significantly higher luciferase expression levels in muscle tissue compared to all other tested polyplex formulations (**Fig. S18**). Based on these results, the 1762 carrier, along with U1 carrier 1611, which displayed a more favorable toxicity profile [52], were selected for the *in vivo* evaluation of polyplexes for Cas9-induced dystrophin modification. Additionally, luciferase mRNA LNP formulations containing either 1621 as cationizable component or, as gold standard, the well-

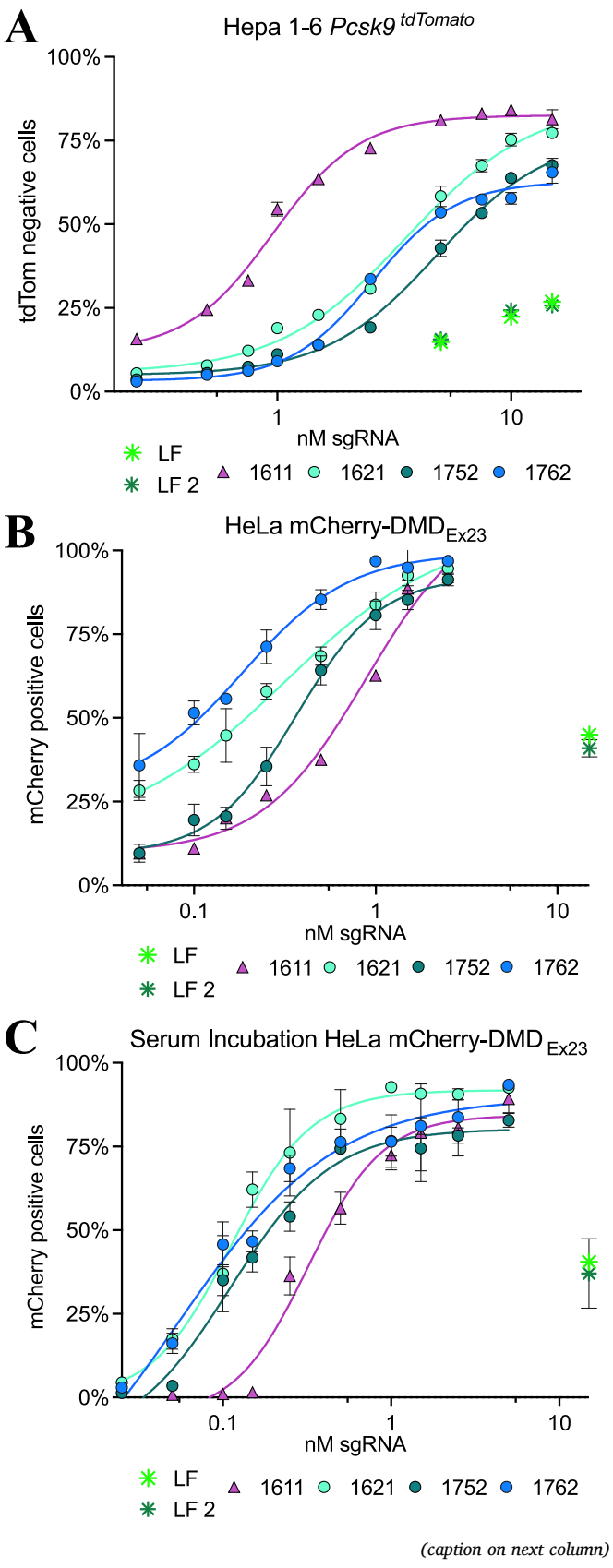

(caption on next column)

Fig. 5. Dose titration of best performing LAF-Stp carriers forming Cas9 polyplexes containing Cas9 mRNA and sgRNA at weight ratio 1:1. N/P ratio of bundle and U1 carriers was 24 and 18, respectively. **(A)** *In vitro* Pcsk9 knock out in Hepa 1–6 *Pcsk9*^{tdTomato} cells treated with 0.25 nM–15 nM sgPcsk9. Positive controls were presented by Lipofectamine™ Messenger MAX™ lipoplexes (LF, LF 2) used for transfection of Cas9 mRNA and sgRNA according to both manufacturer's protocol options resulting in a concentration of 5 nM, 10 nM, and 15 nM sgPCSK9. **(B)** *In vitro* exon skipping evaluation on HeLa mCherry-DMD$_{EX23}$ cells treated with 50 pM – 2.5 nM sgDMD$_{Ex23}$. Positive controls were presented by Lipofectamine™ Messenger MAX™ lipoplexes used for transfection of Cas9 mRNA and sgRNA according to both manufacturer's protocol options resulting in a concentration of 15 nM sgRNA. **(C)** *In vitro* performance of LAF polyplexes in presence of full serum. Samples were diluted in full serum (25 pM– 0.5 nM sgDMD$_{Ex23}$, 98% serum; 1–2.5 nM, 90% serum) and transfected at indicated low doses in HeLa mCHerry-DMD$_{Ex23}$. ($n = 3$, mean ± SD).

established SM-102 lipid were included in the evaluation. Both luciferase mRNA LNPs showed comparable extremely high i.m. luciferase expression of >10^{10} RLU/g muscle, about 10– to 100-fold higher than the polyplex formulations (**Fig. S18**). Notably, luciferase activity at the 6 h time point of investigation remained focused to the injected muscle (**Fig. S19**); activity in other organs of i.m. injected mice was several 100-fold to 1000-fold lower.

Genome editing and mRNA splicing modulation after single or triple intramuscular application of Cas9 polyplexes and Cas9-LNPs in BALB/c mice is displayed in Fig. 7. Single treatment only yielded very low gene editing and splicing modulation. Triple application improved results for all tested formulations, with total gene editing efficiencies of 2.3% - 3.4%, triggering 6.0% - 9.3% splicing modulation (Fig. 7B, C). Interestingly, genome editing and splice modulation efficiencies do not correlate with the relative expression levels of luciferase mRNA. Intramuscularly applied 1762 or 1611 polyplexes mediated slightly higher genome editing and splice modulating than 1621 or SM-102 LNPs, despite their far lower luciferase mRNA potency. Furthermore, comparing the higher genome editing and splice modulation activity in muscle after intravenous administration with the lower activity in local intramuscular injection, an even higher discrepancy with the relative luciferase expression levels (>100-fold higher muscle luciferase expression upon local injection compared with analogous intravenous injection [52,54]) is observed. Apparently, in the current case, efficient mRNA delivery does not present the bottleneck in the genome editing process in total. Additional hurdles, such as the intracellular assembly of sgRNA with the Cas9 protein to form the RNP complex, followed by their nuclear import, must be overcome after the mRNA is translated into Cas9 protein. Utilization of a non-optimized sgRNA sequence with a relatively low on-target activity score of 7.8 [82] might explain the discrepancy. Optimization of the sgRNA sequence or employing a double sgRNA double-cut approach to excise the genomic exon region, presents a potential option for optimizing genome editing.

Controlling the biodistribution and delivering its nucleic acid payload into specific extrahepatic tissues and cell types remains a major hurdle for Cas9 mRNA/sgRNA nanocarriers. In this respect, the observed triggered alternative mRNA splicing with exon 23 skipping in brain tissue and in cardiac and skeletal muscle is noteworthy. Acknowledging the open questions raised by our present study and the utilized mouse model is paramount. Of note, physical delivery of Cas9 mRNA/sgRNA nanoparticles into tissues, which was not studied in the current study, may significantly differ from functional activity. The latter requires productive intracellular uptake, including endosomal escape, translation into Cas9 protein, assembly into sgRNA RNPs, nuclear delivery, and successful genome editing of target cells. Moreover, the uptake mechanisms, including endocytosis, and cellular responses to nanoparticles, are known to vary among species, thereby influencing the efficacy of functional mRNA delivery [83]. Furthermore, while gene editing targeting the dystrophin 23 exon holds significance for the *mdx* mouse model, it is essential to recognize that a hot spot region of

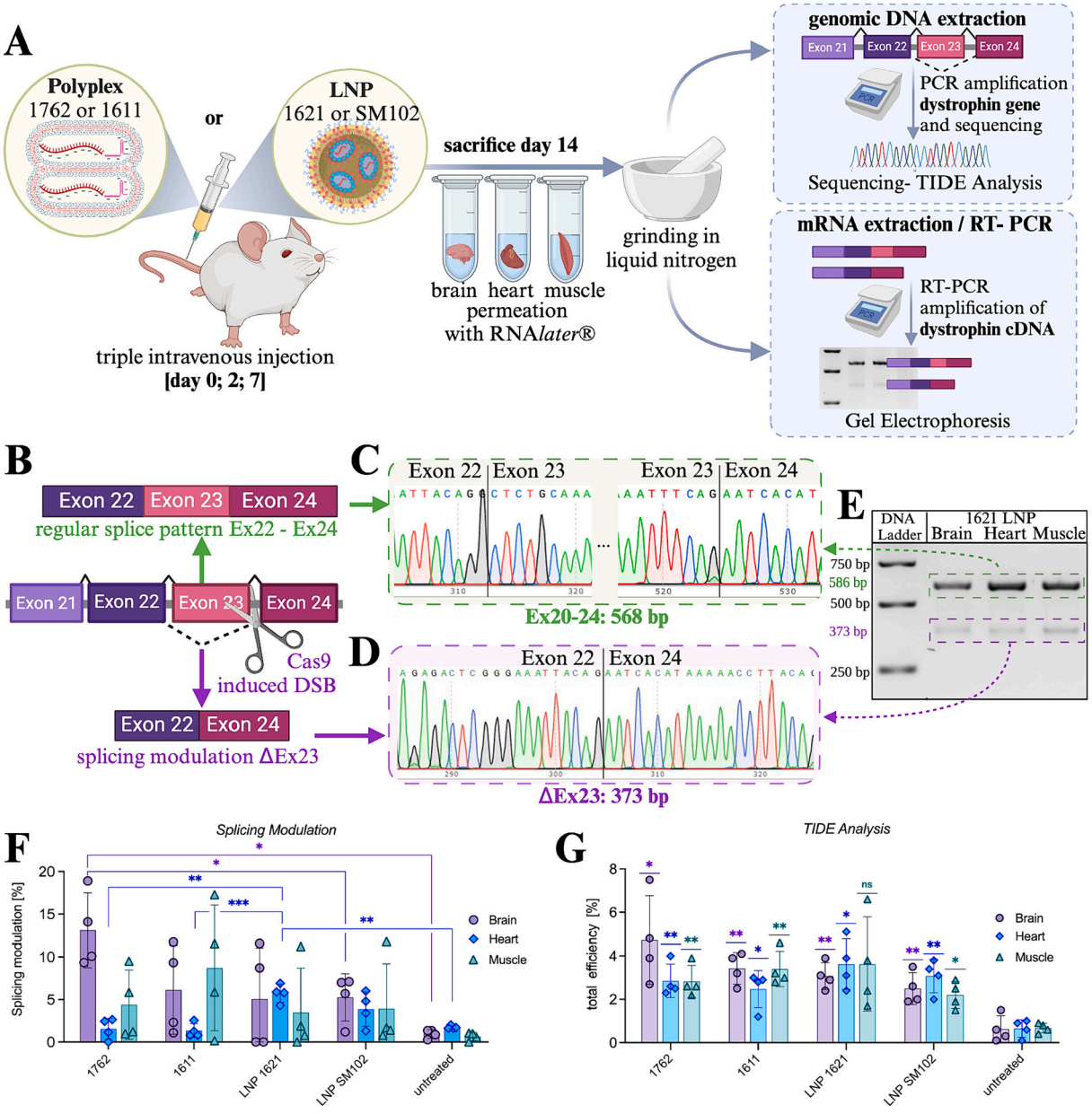

Fig. 6. ***In vivo*** **genome editing and mRNA splicing modulation in BALB/c mice after intravenous injection with Cas9 polyplexes and Cas9 LNPs.** Dystrophin gene editing and mRNA splicing modulation in different organs of BALB/c mice after triple injections of Cas9 polyplexes or Cas9 LNP solution containing Cas9 mRNA and $sgDMD_{Ex23}$ at weight ratio 1:1. All LAF-Stp formulations were compared to LNP containing SM-102 at N/P 6 as gold standard. **(A)** Treatment scheme: triple intravenous injection of 150 µL polyplex or LNP solution containing either 3 µg total RNA in 1762 polyplexes, 1621 LNP and SM-102 LNP or 10 µg total RNA in 1611 polyplexes. Euthanasia at 7 days post last injection, sample preparation and evaluation. Total RNA and genomic DNA was extracted from homogenized dystrophin expressing organs (brain, heart, muscle tissue) at 7 days after last injection. For the evaluation of splicing modulation, a nested RT-PCR was conducted to amplify dystrophin exon 20–24. The RT-PCR product was analyzed on a 2% agarose gel and ratios of splicing modulation were determined using ImageJ Software. For the analysis of the gene editing efficiency a PCR was performed to amplify the region surrounding exon 23. PCR products were purified and sequenced *via* Sanger sequencing. The sequencing results were evaluated using the TIDE (Tracking of Indels by Decomposition) analysis tool. **(B)** Scheme of splicing modulation after of Cas9 induced DSB at donor splice site downstream dystrophin exon 23 **(C)** Sanger sequencing of gel extracted bands corresponding to ~568 bp (complete DMD Ex20–24) **(D)** Sanger sequencing of gel extracted bands corresponding to ~373 bp fragments for confirmation of exon 23 skipping. **(E)** Exemplary gel electrophoresis of RT-PCR products showing splicing modulation in brain, heart, and muscle of animal 1 after triple intravenous treatment with 1621 LNP (N/P 24) containing 3 µg total RNA. **(F)** Evaluation of splicing modulation, as described above, after triple intravenous treatment with either 1762 (N/P 24) polyplexes, 1611 (N/P 18) polyplexes, or LNP 1621 (N/P 24). LNP SM-102 (N/P 6) served as positive control. Individual band intensities were quantified and put into relation to the band of full-length dystrophin exon 20–24 with a size of 568 bp by using the ImageJ software. The complete gel electrophoresis data are provided in **Fig. S17**. **(G)** Evaluation of gene editing efficiency, as described above, after triple intravenous application of 1762 polyplexes, 1621 LNP and SM102 LNP containing 3 µg total RNA and 1611 polyplexes containing 10 µg total RNA. Sanger-sequenced and evaluated by TIDE (Tracking of Indels by Decomposition) analysis. ($n = 4$, mean ± SD). Asterisks indicate statistical significance between treated organ to untreated control. Statistical analysis was performed by unpaired Student's two-tailed *t*-test with Welch's correction; GraphPad Prism™ 10. * $p \leq 0.05$; ** $p \leq 0.01$; *** $p \leq 0.001$; ns, statistically not significant. (For interpretation of the references to colour in this figure legend, the reader is referred to the web version of this article.)

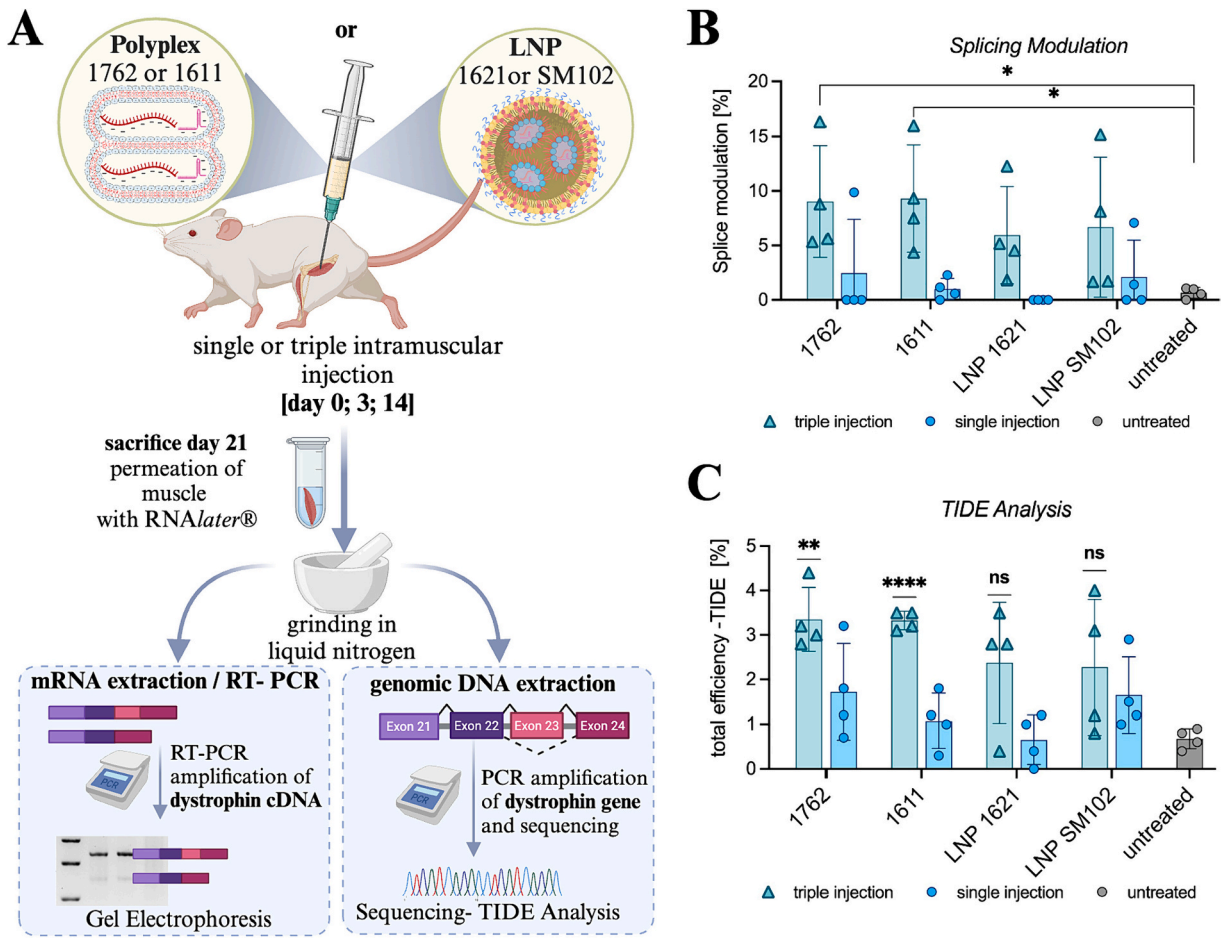

Fig. 7. ***In vivo*** **genome editing and mRNA splicing modulation in BALB/c mice (*n* = 4) after intramuscular injection with Cas9 polyplexes and Cas9 LNPs.** Comparison of dystrophin gene editing and mRNA splicing modulation in muscle tissue of BALB/c mice after single or triple intramuscular injections with polyplexes or Cas9 LNPs containing Cas9 mRNA and $sgDMD_{Ex23}$ at weight ratio 1:1 into the left musculus biceps femoris. Only the tissue of the injected muscle was analyzed after intramuscular application. **(A)** Injection scheme for single or triple intramuscular injection of 50 µL nanocarrier solution containing either 3 µg total RNA in LNP 1621 (N/P 24) and 1762 polyplexes (N/P 24) or 10 µg total RNA in 1611 polyplexes (N/P 18). LNP SM-102 at N/P 6 containing 3 µg total RNA in 50 µL served as gold standard. **(B)** For the evaluation of splicing modulation, a nested RT-PCR was conducted to amplify dystrophin exon 20–24. The RT-PCR product was analyzed on a 2% agarose gel and ratios of splicing modulation were determined using ImageJ Software. The complete gel electrophoresis data are provided in **Fig. S20**. **(C)** Total genomic DNA was extracted from homogenized organs and PCR were conducted to amplify the genomic region surrounding the dystrophin exon 23. PCR products were purified, Sanger-sequenced and evaluated by TIDE (Tracking of Indels by Decomposition) analysis. (n = 4, mean ± SD). Asterisks indicate statistical significance between treated organ to untreated control. Statistical analysis was done by unpaired Student's two-tailed *t*-test with Welch's correction; GraphPad Prism™ 10. * $p \leq 0.05$; ** $p \leq 0.01$; *** $p \leq 0.001$; **** $p \leq 0.0001$; ns, statistically not significant. (For interpretation of the references to colour in this figure legend, the reader is referred to the web version of this article.)

deletions in Duchenne muscular dystrophy is represented by exons 45 to 53. Notably, investigations involving relevant exon 50-deleted mouse and canine models [84,85], alongside a humanized DMD mouse model [40], have been undertaken to assess editing strategies with enhanced translational potential to the human DMD condition.

4. Conclusion

In summary, we evaluated a library of recently reported LAF-Stp lipo-xenopeptides [52,54] for functional delivery of the Cas9 mRNA/sgRNA system. By screening physicochemical nanoparticle properties and functional biological characteristics, xenopeptides 1611 (U-shape topology, Stp/LAF ratio 1:2) and 1762 (B2-topology, Stp/LAF 1:4) containing 12- and 10-aminooctanoic acid LAFs, respectively, were identified as best-performing carriers for Cas9 mRNA/sgRNA polyplexes. Remarkable *in vitro* gene editing efficiency at sub-nanomolar sgRNA concentrations was displayed across various cell lines and reporter target genes. Carrier 1611 also effectively compacted and co-delivered a ssDNA template facilitating up to 38% HDR mediated eGFP to BFP gene conversion. Additionally, a LNP formulation of B2 carrier 1621 was generated. Selected carrier formulations displayed physicochemical and functional stability upon storage at 4 °C and unaffected activity upon incubation in full serum. After intravenous administration in mice, Cas9 mRNA/sgRNA formulations successfully demonstrated *in vivo* genome editing targeting the dystrophin gene exon 23 splice site, thus also triggering alternative mRNA splicing with skipping of exon 23, as observed in cardiac and skeletal muscle and in brain tissue.

CRediT authorship contribution statement

Janin Germer: Writing – review & editing, Writing – original draft, Visualization, Validation, Methodology, Investigation, Formal analysis, Data curation, Conceptualization. **Anna-Lina Lessl:** Writing – review & editing, Methodology, Investigation, Formal analysis, Data curation. **Jana Pöhmerer:** Writing – review & editing, Methodology, Investigation, Formal analysis, Data curation, Conceptualization. **Melina Grau:** Validation, Resources, Methodology, Investigation, Data curation. **Eric**

Weidinger: Writing – review & editing, Validation, Methodology, Investigation. **Miriam Höhn:** Resources, Methodology, Investigation, Formal analysis, Data curation. **Mina Yazdi:** Data curation, Investigation, Formal analysis, Resources, Validation. **Martino Alfredo Cappelluti:** Resources, Methodology, Conceptualization. **Angelo Lombardo:** Writing – review & editing, Supervision, Resources, Methodology, Funding acquisition, Conceptualization. **Ulrich Lächelt:** Writing – review & editing, Validation, Supervision, Conceptualization. **Ernst Wagner:** Writing – review & editing, Writing – original draft, Validation, Supervision, Resources, Project administration, Investigation, Funding acquisition, Formal analysis, Conceptualization.

Declaration of competing interest

None.

Data availability

Data will be made available on request.

Acknowledgements

The authors acknowledge support by the UPGRADE (Unlocking Precision Gene Therapy) project that has received funding from the European Union's Horizon 2020 research and innovation programme under grant agreement No 825825. This work was also supported by the German Research Foundation (DFG) SFB1032 (project-ID 201269156) sub-project B4 (to E.W.), and BMBF Cluster for Future 'CNATM - Cluster for Nucleic Acid Therapeutics Munich' (to E.W.). We thank Ulrich Wilk for his contribution to the animal experiment. We appreciate Wolfgang Rödl and Olga Brück (Pharmaceutical Biotechnology, LMU Munich) for their practical support. Especially, we thank our former animal attendant Markus Kovac for his great contributions to our team in every respect. Graphics in Scheme 1, Figs. 3, 4, 6, 7, S9, S17, S18 and the graphical abstract were created with BioRender.com.

Appendix A. Supplementary data

Supplementary data to this article can be found online at https://doi.org/10.1016/j.jconrel.2024.04.037.

References

[1] A.S.G.C.T. Gene, Cell & RNA Therapy Landscape Report, Q1, 2024.
[2] L. Schoenmaker, D. Witzigmann, J.A. Kulkarni, R. Verbeke, G. Kersten, W. Jiskoot, D.J.A. Crommelin, mRNA-lipid nanoparticle COVID-19 vaccines: structure and stability, Int. J. Pharm. 601 (2021) 120586.
[3] D. Adams, A. Gonzalez-Duarte, W.D. O'Riordan, C.-C. Yang, M. Ueda, A.V. Kristen, I. Tournev, H.H. Schmidt, T. Coelho, J.L. Berk, Patisiran, an RNAi therapeutic, for hereditary transthyretin amyloidosis, New Engl. J. Med. 379 (2018) 11–21.
[4] P.L. Felgner, Y. Barenholz, J.P. Behr, S.H. Cheng, P. Cullis, L. Huang, J.A. Jessee, L. Seymour, F. Szoka, A.R. Thierry, E. Wagner, G. Wu, Nomenclature for synthetic gene delivery systems, Hum. Gene Ther. 8 (1997) 511–512.
[5] Non-viral vectors for gene therapy, Edited by L. Huang, MC. Hung, E. Wagner, Adv. Genet 53 (2005) 1–373, 54, 1–375.
[6] C.Y. Wang, L. Huang, pH-sensitive immunoliposomes mediate target-cell-specific delivery and controlled expression of a foreign gene in mouse, Proc. Natl. Acad. Sci. USA 84 (1987) 7851–7855.
[7] P.L. Felgner, T.R. Gadek, M. Holm, R. Roman, H.W. Chan, M. Wenz, J.P. Northrop, G.M. Ringold, M. Danielsen, Lipofection: a highly efficient, lipid mediated DNA-transfection procedure, Proc. Natl. Acad. Sci. USA 84 (1987) 7413–7417.
[8] G.J. Nabel, E.G. Nabel, Z.Y. Yang, B.A. Fox, G.E. Plautz, X. Gao, L. Huang, S. Shu, D. Gordon, A.E. Chang, Direct gene transfer with DNA-liposome complexes in melanoma: expression, biologic activity, and lack of toxicity in humans, Proc. Natl. Acad. Sci. USA 90 (1993) 11307–11311.
[9] Y. Wang, H.H. Su, Y. Yang, Y. Hu, L. Zhang, P. Blancafort, L. Huang, Systemic delivery of modified mRNA encoding herpes simplex virus 1 thymidine kinase for targeted cancer gene therapy, Mol. Ther. 21 (2013) 358–367.
[10] Y. Sato, K. Hashiba, K. Sasaki, M. Maeki, M. Tokeshi, H. Harashima, Understanding structure-activity relationships of pH-sensitive cationic lipids facilitates the rational identification of promising lipid nanoparticles for delivering siRNAs in vivo, J. Control. Release 295 (2019) 140–152.
[11] P.R. Cullis, M.J. Hope, Lipid nanoparticle systems for enabling gene therapies, Mol. Ther. 25 (2017) 1467–1475.
[12] O.S. Fenton, K.J. Kauffman, J.C. Kaczmarek, R.L. McClellan, S. Jhunjhunwala, M. W. Tibbitt, M.D. Zeng, E.A. Appel, J.R. Dorkin, F.F. Mir, J.H. Yang, M.A. Oberli, M. W. Heartlein, F. DeRosa, R. Langer, D.G. Anderson, Synthesis and biological evaluation of Ionizable lipid materials for the in vivo delivery of messenger RNA to B lymphocytes, Adv. Mater. 29 (2017) 1606944.
[13] S.A. Dilliard, Q. Cheng, D.J. Siegwart, On the mechanism of tissue-specific mRNA delivery by selective organ targeting nanoparticles, Proc. Natl. Acad. Sci. USA 118 (2021) e2109256118.
[14] M. Herrera-Barrera, R.C. Ryals, M. Gautam, A. Jozic, M. Landry, T. Korzun, M. Gupta, C. Acosta, J. Stoddard, R. Reynaga, W. Tschetter, N. Jacomino, O. Taratula, C. Sun, A.K. Lauer, M. Neuringer, G. Sahay, Peptide-guided lipid nanoparticles deliver mRNA to the neural retina of rodents and nonhuman primates, Sci. Adv. 9 (2023) eadd4623.
[15] S.G. Huayamares, M.P. Lokugamage, R. Rab, A.J. Da Silva Sanchez, H. Kim, A. Radmand, D. Loughrey, L. Lian, Y. Hou, B.R. Achyut, A. Ehrhardt, J.S. Hong, C. D. Sago, K. Paunovska, E.S. Echeverri, D. Vanover, P.J. Santangelo, E.J. Sorscher, J. E. Dahlman, High-throughput screens identify a lipid nanoparticle that preferentially delivers mRNA to human tumors in vivo, J. Control. Release 357 (2023) 394–403.
[16] Z. Chen, Y. Tian, J. Yang, F. Wu, S. Liu, W. Cao, W. Xu, T. Hu, D.J. Siegwart, H. Xiong, Modular Design of Biodegradable Ionizable Lipids for improved mRNA delivery and precise Cancer metastasis delineation in vivo, J. Am. Chem. Soc. 145 (2023) 24302–24314.
[17] S. Douka, L.E. Brandenburg, C. Casadidio, J. Walther, B.B.M. Garcia, J. Spanholtz, M. Raimo, W.E. Hennink, E. Mastrobattista, M. Caiazzo, Lipid nanoparticle-mediated messenger RNA delivery for ex vivo engineering of natural killer cells, J. Control. Release 361 (2023) 455–469.
[18] S.C. De Smedt, J. Demeester, W.E. Hennink, Cationic polymer based gene delivery systems, Pharm. Res. 17 (2000) 113–126.
[19] S.M. Zou, P. Erbacher, J.S. Remy, J.P. Behr, Systemic linear polyethylenimine (L-PEI)-mediated gene delivery in the mouse, J. Gene Med. 2 (2000) 128–134.
[20] D.W. Pack, A.S. Hoffman, S. Pun, P.S. Stayton, Design and development of polymers for gene delivery, Nat. Rev. Drug Discov. 4 (2005) 581–593.
[21] M. Breunig, U. Lungwitz, R. Liebl, A. Goepferich, Breaking up the correlation between efficacy and toxicity for nonviral gene delivery, Proc. Natl. Acad. Sci. USA 104 (2007) 14454–14459.
[22] S. Hobel, A. Aigner, Polyethylenimines for siRNA and miRNA delivery in vivo, Wiley Interdiscip. Rev. Nanomed. Nanobiotechnol. 5 (2013) 484–501.
[23] K. Miyata, N. Nishiyama, K. Kataoka, Rational design of smart supramolecular assemblies for gene delivery: chemical challenges in the creation of artificial viruses, Chem. Soc. Rev. 41 (2012) 2562–2574.
[24] I. Martin, C. Dohmen, C. Mas-Moruno, C. Troiber, P. Kos, D. Schaffert, U. Lächelt, M. Teixido, M. Günther, H. Kessler, E. Giralt, E. Wagner, Solid-phase-assisted synthesis of targeting peptide-PEG-oligo(ethane amino)amides for receptor-mediated gene delivery, Org. Biomol. Chem. 10 (2012) 3258–3268.
[25] Q. Leng, S.T. Chou, P.V. Scaria, M.C. Woodle, A.J. Mixson, Increased tumor distribution and expression of histidine-rich plasmid polyplexes, J. Gene Med. 16 (2014) 317–328.
[26] C. Goncalves, S. Akhter, C. Pichon, P. Midoux, Intracellular availability of pDNA and mRNA after transfection: a comparative study among Polyplexes, Lipoplexes, and Lipopolyplexes, Mol. Pharm. 13 (2016) 3153–3163.
[27] M. Chiper, N. Tounsi, R. Kole, A. Kichler, G. Zuber, Self-aggregating 1.8kDa polyethylenimines with dissolution switch at endosomal acidic pH are delivery carriers for plasmid DNA, mRNA, siRNA and exon-skipping oligonucleotides, J. Control. Release 246 (2017) 60–70.
[28] D.P. Feldmann, Y. Cheng, R. Kandil, Y. Xie, M. Mohammadi, H. Harz, A. Sharma, D. J. Peeler, A. Moszczynska, H. Leonhardt, S.H. Pun, O.M. Merkel, In vitro and in vivo delivery of siRNA via VIPER polymer system to lung cells, J. Control. Release 276 (2018) 50–58.
[29] S. Abbasi, S. Uchida, K. Toh, T.A. Tockary, A. Dirisala, K. Hayashi, S. Fukushima, K. Kataoka, Co-encapsulation of Cas9 mRNA and guide RNA in polyplex micelles enables genome editing in mouse brain, J. Control. Release 332 (2021) 260–268.
[30] M. Karimov, M. Schulz, T. Kahl, S. Noske, M. Kubczak, I. Gockel, R. Thieme, T. Büch, A. Reinert, M. Ionov, M. Bryszewska, H. Franke, U. Krügel, A. Ewe, A. Aigner, Tyrosine-modified linear PEIs for highly efficacious and biocompatible siRNA delivery in vitro and in vivo, Nanomed 36 (2021) 102403.
[31] A. Dirisala, S. Uchida, J. Li, J.F.R. Van Guyse, K. Hayashi, S.V.C. Vummaleti, S. Kaur, Y. Mochida, S. Fukushima, K. Kataoka, Effective mRNA protection by poly (l-ornithine) synergizes with endosomal escape functionality of a charge-conversion polymer toward maximizing mRNA introduction efficiency, Macromol. Rapid Commun. 43 (2022) e2100754.
[32] U. Lächelt, E. Wagner, Nucleic acid therapeutics using Polyplexes: a journey of 50 years (and beyond), Chem. Rev. 115 (2015) 11043–11078.
[33] R. Kumar, C.F. Santa Chalarca, M.R. Bockman, C.V. Bruggen, C.J. Grimme, R. J. Dalal, M.G. Hanson, J.K. Hexum, T.M. Reineke, Polymeric delivery of therapeutic nucleic acids, Chem. Rev. 121 (2021) 11527–11652.
[34] T. Bus, A. Traeger, U.S. Schubert, The great escape: how cationic polyplexes overcome the endosomal barrier, J. Mater. Chem. B 6 (2018) 6904–6918.
[35] L. Peng, E. Wagner, Polymeric carriers for nucleic acid delivery: current designs and future directions, Biomacromol 20 (2019) 3613–3626.
[36] B. Winkeljann, D.C. Keul, O.M. Merkel, Engineering poly- and micelleplexes for nucleic acid delivery - a reflection on their endosomal escape, J. Control. Release 353 (2023) 518–534.

[37] S.N. Bhatia, J.E. Dahlman, RNA delivery systems, Proc. Natl. Acad. Sci. USA 121 (2024) e2315789121.
[38] J. Witten, Y. Hu, R. Langer, D.G. Anderson, Recent advances in nanoparticulate RNA delivery systems, Proc. Natl. Acad. Sci. USA 121 (2024) e2307798120.
[39] S. Berger, U. Lächelt, E. Wagner, Dynamic carriers for therapeutic RNA delivery, Proc. Natl. Acad. Sci. USA 121 (2024) e2307799120.
[40] E. Kenjo, H. Hozumi, Y. Makita, K.A. Iwabuchi, N. Fujimoto, S. Matsumoto, M. Kimura, Y. Amano, M. Ifuku, Y. Naoe, Low immunogenicity of LNP allows repeated administrations of CRISPR-Cas9 mRNA into skeletal muscle in mice, Nat. Commun. 12 (2021) 7101.
[41] C. Wong, UK first to approve CRISPR treatment for diseases: what you need to know, Nature 623 (2023) 676–677.
[42] H. Frangoul, D. Altshuler, M.D. Cappellini, Y.-S. Chen, J. Domm, B.K. Eustace, J. Foell, J. de la Fuente, S. Grupp, R. Handgretinger, CRISPR-Cas9 gene editing for sickle cell disease and β-thalassemia, New Engl. J. Med. 384 (2021) 252–260.
[43] J.D. Gillmore, E. Gane, J. Taubel, J. Kao, M. Fontana, M.L. Maitland, J. Seitzer, D. O'Connell, K.R. Walsh, K. Wood, CRISPR-Cas9 in vivo gene editing for transthyretin amyloidosis, New Engl. J. Med. 385 (2021) 493–502.
[44] Y. Lin, E. Wagner, U. Lächelt, Non-viral delivery of the CRISPR/Cas system: DNA versus RNA versus RNP, Biomater. Sci. 10 (2022) 1166–1192.
[45] C.A. Tsuchida, K.M. Wasko, J.R. Hamilton, J.A. Doudna, Targeted nonviral delivery of genome editors in vivo, Proc. Natl. Acad. Sci. USA 121 (2024) e2307796121.
[46] J. Walther, D. Porenta, D. Wilbie, C. Seinen, N. Benne, Q. Yang, O.G. de Jong, Z. Lei, E. Mastrobattista, Comparative analysis of lipid nanoparticle-mediated delivery of CRISPR-Cas9 RNP versus mRNA/sgRNA for gene editing in vitro and in vivo, Eur. J. Pharm. Biopharm. 196 (2024) 114207.
[47] L. Farbiak, Q. Cheng, T. Wei, E. Álvarez-Benedicto, L.T. Johnson, S. Lee, D. J. Siegwart, All-in-one dendrimer-based lipid nanoparticles enable precise HDR-mediated Gene editing in vivo, Adv. Mater. 33 (2021) e2006619.
[48] T. Wei, Q. Cheng, Y.L. Min, E.N. Olson, D.J. Siegwart, Systemic nanoparticle delivery of CRISPR-Cas9 ribonucleoproteins for effective tissue specific genome editing, Nat. Commun. 11 (2020) 3232.
[49] F. Freitag, E. Wagner, Optimizing synthetic nucleic acid and protein nanocarriers: the chemical evolution approach, Adv. Drug Deliv. Rev. 168 (2021) 30–54.
[50] Y. Lin, X. Luo, T. Burghardt, S. Dorrer, M. Höhn, E. Wagner, U. Lächelt, Chemical evolution of amphiphilic Xenopeptides for potentiated Cas9 ribonucleoprotein delivery, J. Am. Chem. Soc. 145 (2023) 15171–15179.
[51] Y. Lin, U. Wilk, J. Pöhmerer, E. Hörterer, M. Höhn, X. Luo, H. Mai, E. Wagner, U. Lächelt, Folate receptor-mediated delivery of Cas9 RNP for enhanced immune checkpoint disruption in Cancer cells, Small 19 (2023) 2205318.
[52] S. Thalmayr, M. Grau, L. Peng, J. Pöhmerer, U. Wilk, P. Folda, M. Yazdi, E. Weidinger, T. Burghardt, M. Höhn, E. Wagner, S. Berger, Molecular chameleon carriers for nucleic acid delivery: the sweet spot between Lipoplexes and Polyplexes, Adv. Mater. 35 (2023) e2211105.
[53] C. Scholz, E. Wagner, Therapeutic plasmid DNA versus siRNA delivery: common and different tasks for synthetic carriers, J. Control. Release 161 (2012) 554–565.
[54] F. Haase, J. Pöhmerer, M. Yazdi, M. Grau, Y. Zeyn, U. Wilk, T. Burghardt, M. Höhn, C. Hieber, M. Bros, E. Wagner, S. Berger, Lipoamino bundle LNPs for efficient mRNA transfection of dendritic cells and macrophages show high spleen selectivity, Eur. J. Pharm. Biopharm. 194 (2024) 95–109.
[55] H. Yin, C.Q. Song, S. Suresh, Q. Wu, S. Walsh, L.H. Rhym, E. Mintzer, M. F. Bolukbasi, L.J. Zhu, K. Kauffman, H. Mou, A. Oberholzer, J. Ding, S.Y. Kwan, R. L. Bogorad, T. Zatsepin, V. Koteliansky, S.A. Wolfe, W. Xue, R. Langer, D. G. Anderson, Structure-guided chemical modification of guide RNA enables potent non-viral in vivo genome editing, Nat. Biotechnol. 35 (2017) 1179–1187.
[56] M.A. Cappelluti, V. Mollica Poeta, S. Valsoni, P. Quarato, S. Merlin, I. Merelli, A. Lombardo, Durable and efficient gene silencing in vivo by hit-and-run epigenome editing, Nature 627 (2024) 416–423.
[57] J. Kuhn, Y. Lin, A. Krhac Levacic, N. Al Danaf, L. Peng, M. Höhn, D.C. Lamb, E. Wagner, U. Lächelt, Delivery of Cas9/sgRNA ribonucleoprotein complexes via Hydroxystearyl Oligoamino amides, Bioconjug. Chem. 31 (2020) 729–742.
[58] A. Zintchenko, A. Philipp, A. Dehshahri, E. Wagner, Simple modifications of branched PEI Lead to highly efficient siRNA carriers with low toxicity, Bioconjug. Chem. 19 (2008) 1448–1455.
[59] Q. Cheng, T. Wei, Y. Jia, L. Farbiak, K. Zhou, S. Zhang, Y. Wei, H. Zhu, D. J. Siegwart, Dendrimer-based lipid nanoparticles deliver therapeutic FAH mRNA to normalize liver function and extend survival in a mouse model of hepatorenal tyrosinemia type I, Adv. Mater. 30 (2018) 1805308.
[60] A. Lombardo, D. Cesana, P. Genovese, B. Di Stefano, E. Provasi, D.F. Colombo, M. Neri, Z. Magnani, A. Cantore, P.L. Riso, Site-specific integration and tailoring of cassette design for sustainable gene transfer, Nat. Methods 8 (2011) 861–869.
[61] A.L. Lessl, J. Pöhmerer, Y. Lin, U. Wilk, M. Höhn, E. Hörterer, E. Wagner, U. Lächelt, mCherry on top: a positive read-out cellular platform for screening DMD exon skipping Xenopeptide-PMO conjugates, Bioconjug. Chem. 34 (2023) 2263–2274.
[62] L. Farbiak, Q. Cheng, T. Wei, E. Álvarez-Benedicto, L.T. Johnson, S. Lee, D. J. Siegwart, All-in-one dendrimer-based lipid nanoparticles enable precise HDR-mediated gene editing in vivo, Adv. Mater. 33 (2021) 2006619.
[63] S.M. Hammond, G. McClorey, J.Z. Nordin, C. Godfrey, S. Stenler, K.A. Lennox, C. I. Smith, A.M. Jacobi, M.A. Varela, Y. Lee, M.A. Behlke, M.J. Wood, S. E. Andaloussi, Correlating in vitro splice switching activity with systemic in vivo delivery using novel ZEN-modified oligonucleotides, Mol Ther Nucleic Acids 3 (2014) e212.
[64] P. Gee, M.S. Lung, Y. Okuzaki, N. Sasakawa, T. Iguchi, Y. Makita, H. Hozumi, Y. Miura, L.F. Yang, M. Iwasaki, Extracellular nanovesicles for packaging of CRISPR-Cas9 protein and sgRNA to induce therapeutic exon skipping, Nat. Commun. 11 (2020) 1334.
[65] H. Yin, H.M. Moulton, Y. Seow, C. Boyd, J. Boutilier, P. Iverson, M.J. Wood, Cell-penetrating peptide-conjugated antisense oligonucleotides restore systemic muscle and cardiac dystrophin expression and function, Hum. Mol. Genet. 17 (2008) 3909–3918.
[66] E.K. Brinkman, T. Chen, M. Amendola, B. Van Steensel, Easy quantitative assessment of genome editing by sequence trace decomposition, Nucleic Acids Res. 42 (2014) e168.
[67] E.K. Brinkman, B. van Steensel, Rapid quantitative evaluation of CRISPR genome editing by TIDE and TIDER, in: Y. Luo (Ed.), CRISPR Gene Editing: Methods and Protocols, Springer, New York, New York, NY, 2019, pp. 29–44.
[68] D. Schaffert, N. Badgujar, E. Wagner, Novel Fmoc-polyamino acids for solid-phase synthesis of defined polyamidoamines, Org. Lett. 13 (2011) 1586–1589.
[69] D. Schaffert, C. Troiber, E.E. Salcher, T. Frohlich, I. Martin, N. Badgujar, C. Dohmen, D. Edinger, R. Klager, G. Maiwald, K. Farkasova, S. Seeber, K. Jahn-Hofmann, P. Hadwiger, E. Wagner, Solid-phase synthesis of sequence-defined T-, i-, and U-shape polymers for pDNA and siRNA delivery, Angew. Chem. Int. Ed. Eng. 50 (2011) 8986–8989.
[70] J.D. Finn, A.R. Smith, M.C. Patel, L. Shaw, M.R. Youniss, J. van Heteren, T. Dirstine, C. Ciullo, R. Lescarbeau, J. Seitzer, R.R. Shah, A. Shah, D. Ling, J. Growe, M. Pink, E. Rohde, K.M. Wood, W.E. Salomon, W.F. Harrington, C. Dombrowski, W.R. Strapps, Y. Chang, D.V. Morrissey, A single administration of CRISPR/Cas9 lipid nanoparticles achieves robust and persistent in vivo genome editing, Cell Rep. 22 (2018) 2227–2235.
[71] K. Von Gersdorff, N.N. Sanders, R. Vandenbroucke, S.C. De Smedt, E. Wagner, M. Ogris, The internalization route resulting in successful gene expression depends on both cell line and polyethylenimine polyplex type, Mol. Ther. 14 (2006) 745–753.
[72] A.K. Levačić, S. Berger, J. Müller, A. Wegner, U. Lächelt, C. Dohmen, C. Rudolph, E. Wagner, Dynamic mRNA polyplexes benefit from bioreducible cleavage sites for in vitro and in vivo transfer, J. Control. Release 339 (2021) 27–40.
[73] C. Long, L. Amoasii, A.A. Mireault, J.R. McAnally, H. Li, E. Sanchez-Ortiz, S. Bhattacharyya, J.M. Shelton, R. Bassel-Duby, E.N. Olson, Postnatal genome editing partially restores dystrophin expression in a mouse model of muscular dystrophy, Science 351 (2016) 400–403.
[74] F. Chemello, E.N. Olson, R. Bassel-Duby, CRISPR-editing therapy for Duchenne muscular dystrophy, Hum. Gene Ther. 34 (2023) 379–387.
[75] M. Kosicki, F. Allen, F. Steward, K. Tomberg, Y. Pan, A. Bradley, Cas9-induced large deletions and small indels are controlled in a convergent fashion, Nat. Commun. 13 (2022) 3422.
[76] M. Kosicki, K. Tomberg, A. Bradley, Repair of double-strand breaks induced by CRISPR–Cas9 leads to large deletions and complex rearrangements, Nat. Biotechnol. 36 (2018) 765–771.
[77] S. Berger, M. Berger, C. Bantz, M. Maskos, E. Wagner, Performance of nanoparticles for biomedical applications: the in vitro/in vivo discrepancy, Biophys. Rev. 3 (2022).
[78] K. Paunovska, C.D. Sago, C.M. Monaco, W.H. Hudson, M.G. Castro, T.G. Rudoltz, S. Kalathoor, D.A. Vanover, P.J. Santangelo, R. Ahmed, A direct comparison of in vitro and in vivo nucleic acid delivery mediated by hundreds of nanoparticles reveals a weak correlation, Nano Lett. 18 (2018) 2148–2157.
[79] Q. Cheng, T. Wei, L. Farbiak, L.T. Johnson, S.A. Dilliard, D.J. Siegwart, Selective organ targeting (SORT) nanoparticles for tissue-specific mRNA delivery and CRISPR–Cas gene editing, Nat. Nanotechnol. 15 (2020) 313–320.
[80] M.V. Petkova, S. Morales-Gonzales, K. Relizani, E. Gill, F. Seifert, J. Radke, W. Stenzel, L. Garcia, H. Amthor, M. Schuelke, Characterization of a Dmd EGFP reporter mouse as a tool to investigate dystrophin expression, Skelet. Muscle 6 (2016) 1–16.
[81] R.M. Daer, J.P. Cutts, D.A. Brafman, K.A. Haynes, The impact of chromatin dynamics on Cas9-mediated genome editing in human cells, ACS Synth. Biol. 6 (2017) 428–438.
[82] J.G. Doench, E. Hartenian, D.B. Graham, Z. Tothova, M. Hegde, I. Smith, M. Sullender, B.L. Ebert, R.J. Xavier, D.E. Root, Rational design of highly active sgRNAs for CRISPR-Cas9–mediated gene inactivation, Nat. Biotechnol. 32 (2014) 1262–1267.
[83] M.Z. Hatit, M.P. Lokugamage, C.N. Dobrowolski, K. Paunovska, H. Ni, K. Zhao, D. Vanover, J. Beyersdorf, H.E. Peck, D. Loughrey, Species-dependent in vivo mRNA delivery and cellular responses to nanoparticles, Nat. Nanotechnol. 17 (2022) 310–318.
[84] L. Amoasii, C. Long, H. Li, A.A. Mireault, J.M. Shelton, E. Sanchez-Ortiz, J. R. McAnally, S. Bhattacharyya, F. Schmidt, D. Grimm, Single-cut genome editing restores dystrophin expression in a new mouse model of muscular dystrophy, Sci. Transl. Med. 9 (2017) eaan8081.
[85] L. Amoasii, J.C. Hildyard, H. Li, E. Sanchez-Ortiz, A. Mireault, D. Caballero, R. Harron, T.-R. Stathopoulou, C. Massey, J.M. Shelton, Gene editing restores dystrophin expression in a canine model of Duchenne muscular dystrophy, Science 362 (2018) 86–91.